Aeroballistic Evaluation of Kinetic Energy (KE) Penetrators for Electromagnetic (EM) Gun Applications

Peter Plostins
Keith P. Soencksen
Alexander E. Zielinski
U.S. ARMY RESEARCH LABORATORY

Tim Hayden
KAMAN SCIENCES CORPORATION

19960124 123

DTIC QUALITY INSPECTED 1

NOTICES

Destroy this report when it is no longer needed. DO NOT return it to the originator.

Additional copies of this report may be obtained from the National Technical Information Service, U.S. Department of Commerce, 5285 Port Royal Road, Springfield, VA 22161.

The findings of this report are not to be construed as an official Department of the Army position, unless so designated by other authorized documents.

The use of trade names or manufacturers' names in this report does not constitute indorsement of any commercial product.

REPORT DOCUMENTATION PAGE

1. AGENCY USE ONLY (Leave blank)	2. REPORT DATE	3. REPORT TYPE AND DATES COVERED
	January 1996	Final, Oct 93–Oct 95

4. TITLE AND SUBTITLE

Aeroballistic Evaluation of Kinetic Energy (KE) Penetrators for Electromagnetic (EM) Gun Applications

5. FUNDING NUMBERS

PR: 1L162618AH80

6. AUTHOR(S)

Peter Plostins, Keith P. Soencksen, Alexander E. Zielinski, and Tim Hayden*

7. PERFORMING ORGANIZATION NAME(S) AND ADDRESS(ES)

U.S. Army Research Laboratory
ATTN: AMSRL-WT-PB
Aberdeen Proving Ground, MD 21005-5066

8. PERFORMING ORGANIZATION REPORT NUMBER

ARL-TR-922

9. SPONSORING/MONITORING AGENCY NAME(S) AND ADDRESS(ES)

10. SPONSORING/MONITORING AGENCY REPORT NUMBER

11. SUPPLEMENTARY NOTES

*Kaman Sciences Corporation, 1500 Garden of the Gods Rd., Colorado Springs, CO 80933-7463.

12a. DISTRIBUTION/AVAILABILITY STATEMENT

Approved for public release; distribution is unlimited.

12b. DISTRIBUTION CODE

13. ABSTRACT (Maximum 200 words)

Aeroballistic tests of candidate penetrator designs for the Cannon Caliber Electromagnetic Gun Program were performed at the U.S. Army Research Laboratory (ARL) Aerodynamics Range Facility. The penetrator configurations were designed by Kaman Sciences Corporation (KSC) under subcontract to United Defense LP. Three candidate penetrator configurations were tested to determine aerodynamic performance. The testing was completed in two phases. An all-steel monoblock fluted flare-stabilized penetrator with driving threads was evaluated in Phase I. Considering the Phase I result, a redesign was initiated and two final designs were proposed and evaluated in Phase II. The final two configurations consisted of a fluted flare design with an improved center-of-gravity location and a cruciform fin-stabilized design. Both final configurations had the driving threads replaced with driving buttress grooves along the length of the body. Phase I testing indicated that the fluted flare design with the threaded body had nonlinear aerodynamic coefficients and a low-static margin, appeared dynamically unstable at moderate angles of attack, and exhibited significant aerodynamic jump sensitivity. Phase II testing of the improved center-of-gravity fluted flare design showed improvements in static margin and drag, but the aerodynamics remained essentially nonlinear. The cruciform tail configuration had a significantly higher static margin, had linear aerodynamics, and was dynamically stable, but had slightly higher drag than the fluted flare design. The cruciform tail design was chosen to be the penetrator for the Cannon Caliber Electromagnetic Gun Program.

14. SUBJECT TERMS

electromagnetic gun, kinetic energy penetrator, fin-stabilized design

15. NUMBER OF PAGES
47

16. PRICE CODE

17. SECURITY CLASSIFICATION OF REPORT	18. SECURITY CLASSIFICATION OF THIS PAGE	19. SECURITY CLASSIFICATION OF ABSTRACT	20. LIMITATION OF ABSTRACT
UNCLASSIFIED	UNCLASSIFIED	UNCLASSIFIED	UL

INTENTIONALLY LEFT BLANK.

TABLE OF CONTENTS

INTENTIONALLY LEFT BLANK.

LIST OF FIGURES

LIST OF TABLES

INTENTIONALLY LEFT BLANK.

1. INTRODUCTION

1.1 <u>Overview of the Program</u>. The Cannon Caliber Electromagnetic Gun (CCEMG) program is managed by the Close Combat Armaments Center (CCAC) of the U.S. Army Armament Research, Development, and Engineering Center (ARDEC), Picatinny Arsenal, New Jersey. The program is supported by the U.S. Army and the U.S. Marine Corps to develop future cannon-caliber armaments for their lightly armored vehicles. Currently the primary armament for vehicles such as the Bradley Fighting Vehicle is a 25-mm M242 Bushmaster chain gun. The CCEMG program is tasked to manufacture a prototype cannon-caliber EM gun system and to develop expertise in electromagnetic (EM) propulsion, cannon, sabot, and projectile design. The prime contractor for this task is United Defense LP, with primary subcontractors Kaman Sciences Corporation (KSC), and the Center for Electromechanics (UT-CEM) at the University of Texas, Austin, Texas.

KSC is responsible for the Integrated Launch Package (ILP) that includes the kinetic energy (KE) penetrator and sabot/armature. They had proposed a fluted flare-stabilized penetrator design shown in Figure 1. The CCAC of ARDEC tasked the U.S. Army Research Laboratory (ARL) with aeroballistic testing of the design. This would provide KSC with experimental data on the performance of the proposed penetrator configuration.

1.2 <u>Initial Considerations</u>. The Aerodynamics Branch of the Weapons Technology Directorate, ARL, could not test the full-scale configuration at the desired Mach number of 5.5 in the Aerodynamics Range Facility. It was resolved to evaluate 3/5-scale models of the penetrator. The subscale penetrator was approximately 5 mm in diameter with an L/D ratio of 21. A powder gun was used in the test since there was previous experience launching KE penetrators at high velocities from powder gun systems. In order to launch the subscale projectile, a high-pressure, high-velocity T-69 20-mm smoothbore cannon was required. This system has launched projectiles of various masses to velocities greater than 2 km/s. The desired velocity for the KSC design was 1,850 m/s. The T-69 gun system can launch an 80-g mass at the desired velocity using a base-pushed sabot system. Interior ballistic calculations using Anderson and Fickie (1987) indicated the peak in-bore acceleration for this sabot/penetrator mass would be approximately 200,000 times the acceleration of gravity.

The full-scale KSC penetrator is designed for midbody sabot drive and uses a titanium rear stabilizer assembly as shown in Figure 1. Structural calculations indicated that the tail assembly might not survive

1

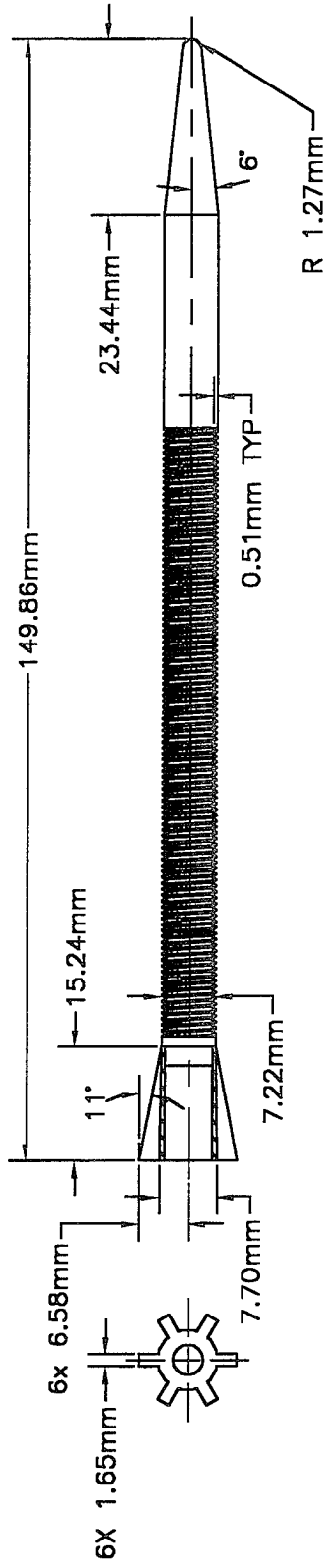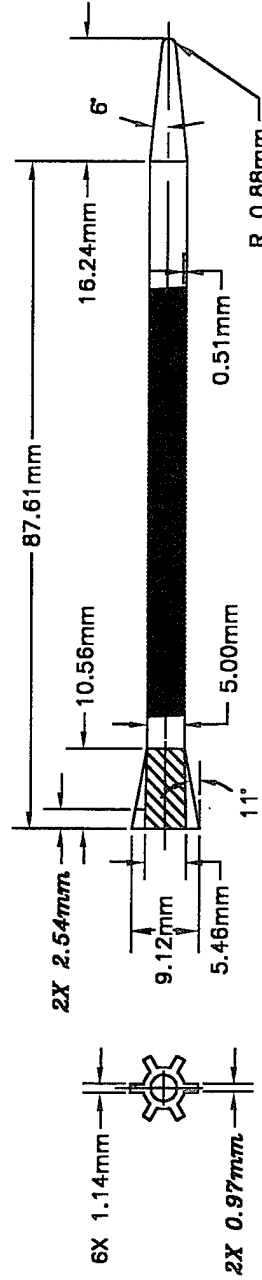Figure 1. Full-scale, fluted, flare-stabilized KE penetrator design.

Figure 2. Subscale, fluted, flare-stabilized KE penetrator design (Phase I test projectile; monoblock maraging steel body).

*Dimensions in italics
define 4 degree roll cants*

peak launch loads using the base-pushed sabot. ARL decided to be conservative and manufacture the subscale penetrator entirely of maraging steel. The sabot pusher was also fabricated of maraging steel whereas the obturator and sabot petals were fabricated from Nylon 6-6. A schematic of the projectile and the sabot system is shown in Figures 2 and 3, respectively. A second reason for being conservative was that there was only one T-69 20-mm smoothbore cannon in the ARL inventory. Structural in-bore failure could have damaged or destroyed the tube, resulting in schedule delays to any other programs requiring this gun system.

ARL was responsible for the manufacture of both the subscale penetrator and the sabot packages. Six subscale penetrators and sabots were needed for aeroballistic testing. Extra penetrators and sabots were manufactured for initial testing to confirm structural integrity of the launch system. The design was a success, and Figures 4 and 5 are x-ray images of the launch of the first subscale design at Mach 5.3 taken 0.22 and 0.85 m from the gun muzzle. Clearly the sabot system is intact and beginning to separate. The maraging steel pusher and penetrator are clearly visible in Figure 5, as is the pin in the base used to measure the penetrator roll orientation. This initial testing also allowed the sabot system to be optimized. The sabot was fabricated from a monoblock cylinder. The drawing in Figure 3 shows the scallops in the sabot petals where the mass was removed to reduce the launch mass. The total launch mass was reduced to 56 g, thus allowing a reduction of the charge mass. For the reduced sabot mass, the peak load was recomputed to be approximately 140,000 g's. No structural problems were ever observed, and this sabot launch system was used throughout both phases of testing. X-ray data taken on all shots indicated low yaw launches had been achieved.

With the launch system design confirmed, the actual aeroballistic testing was then conducted in two phases. Phase I tested the first fluted-flare, subscale configuration shown in Figure 2. The second and third designs were evaluated in Phase II. The details of the procedure, test setup, analysis methodology, and results for both phases of the program are given as follows.

2. TEST SETUP, PROCEDURES, AND DATA ANALYSIS TECHNIQUES

A schematic of the test setup is given in Figure 6. This is the standard system for aeroballistic testing in the ARL Aerodynamics Range Facility. The facility is designed to evaluate the transitional ballistics and the complete aeroballistics of projectiles. Projectiles up to 40 mm in diameter can be tested in the facility. Six orthogonal x-rays are used to determine structural integrity and launch dynamics of
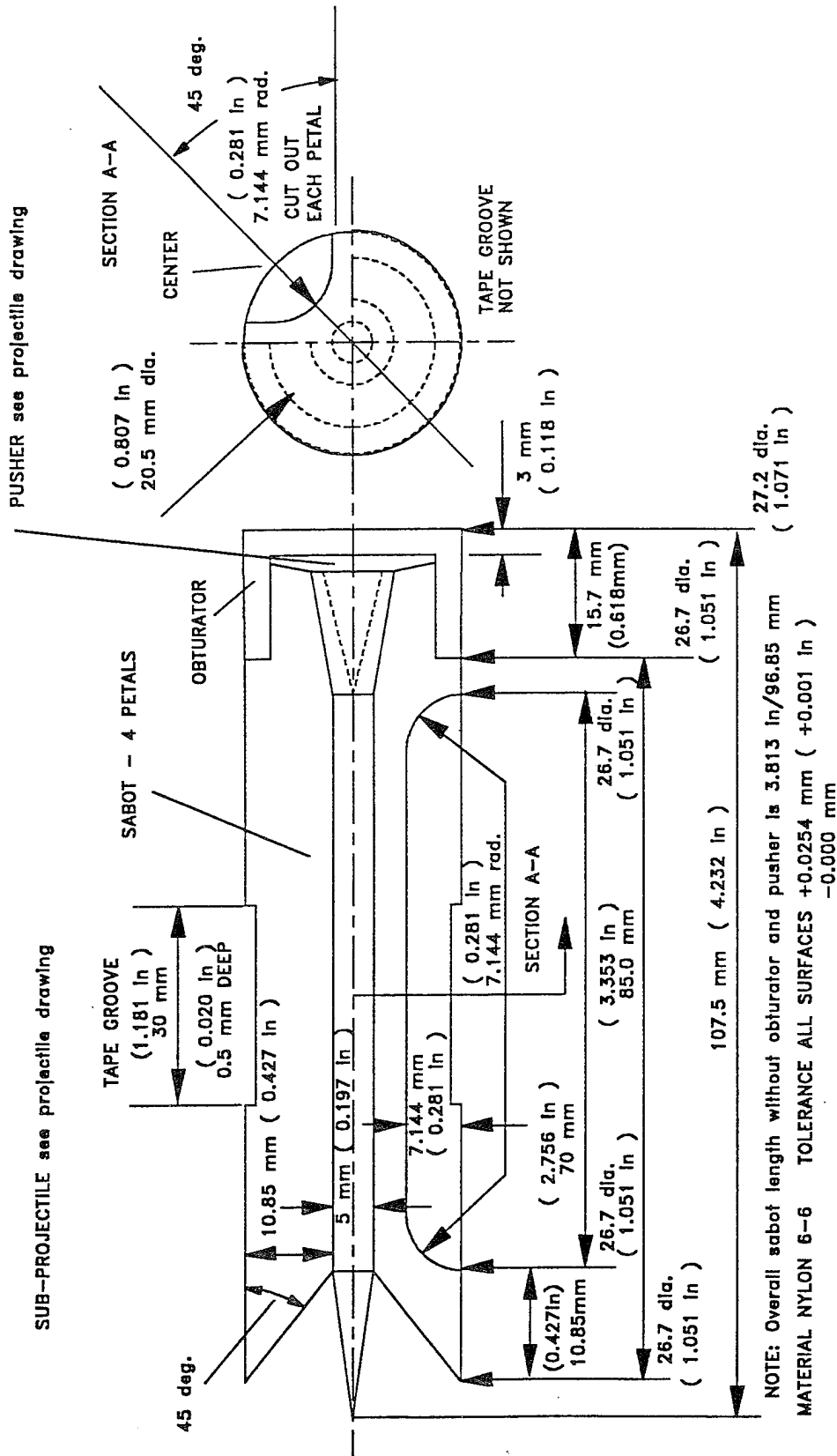
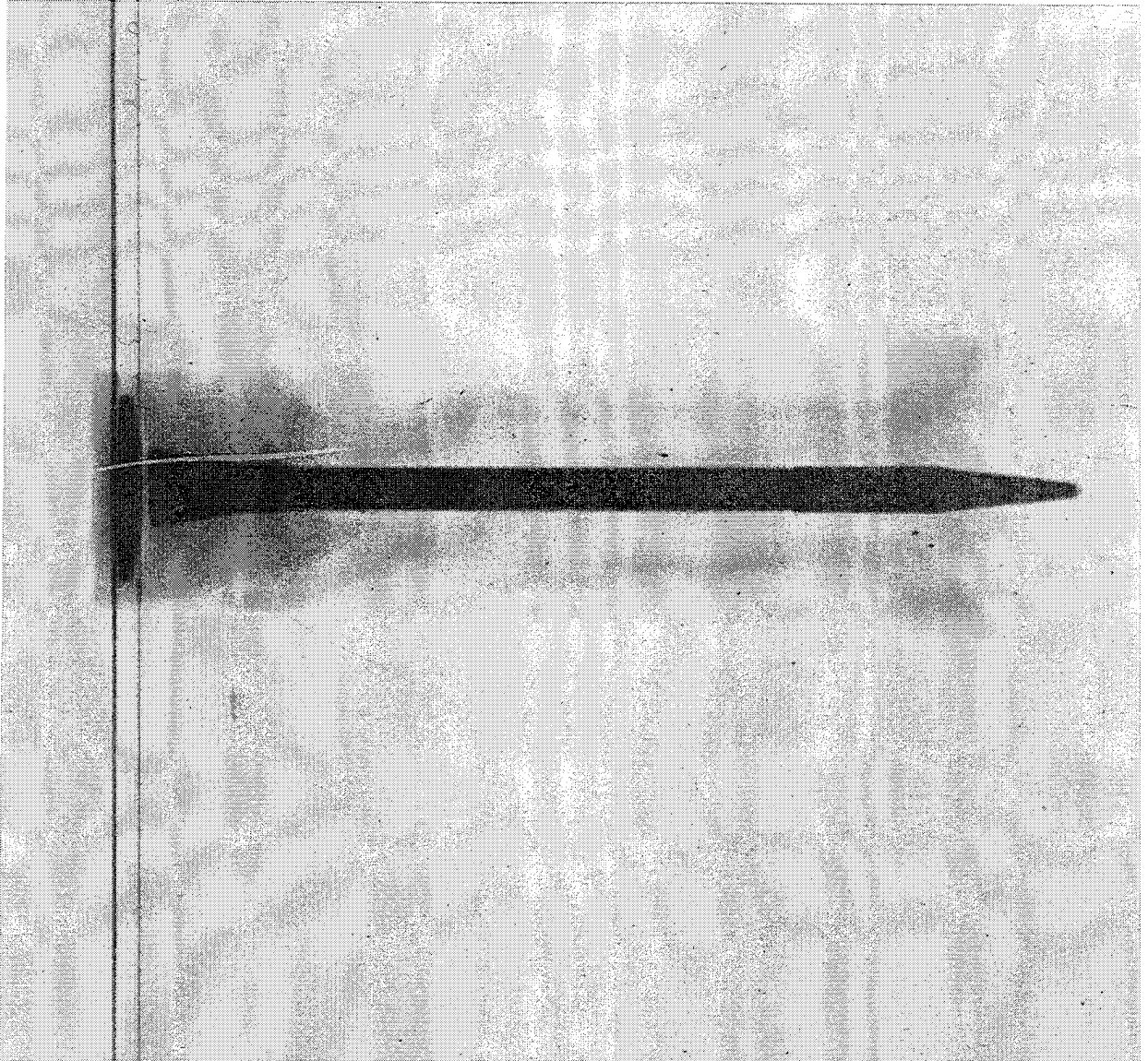Figure 3.   Schematic of the base-pushed sabot assembly.

4

Figure 4. <u>X-ray of the sabot discard and structural integrity
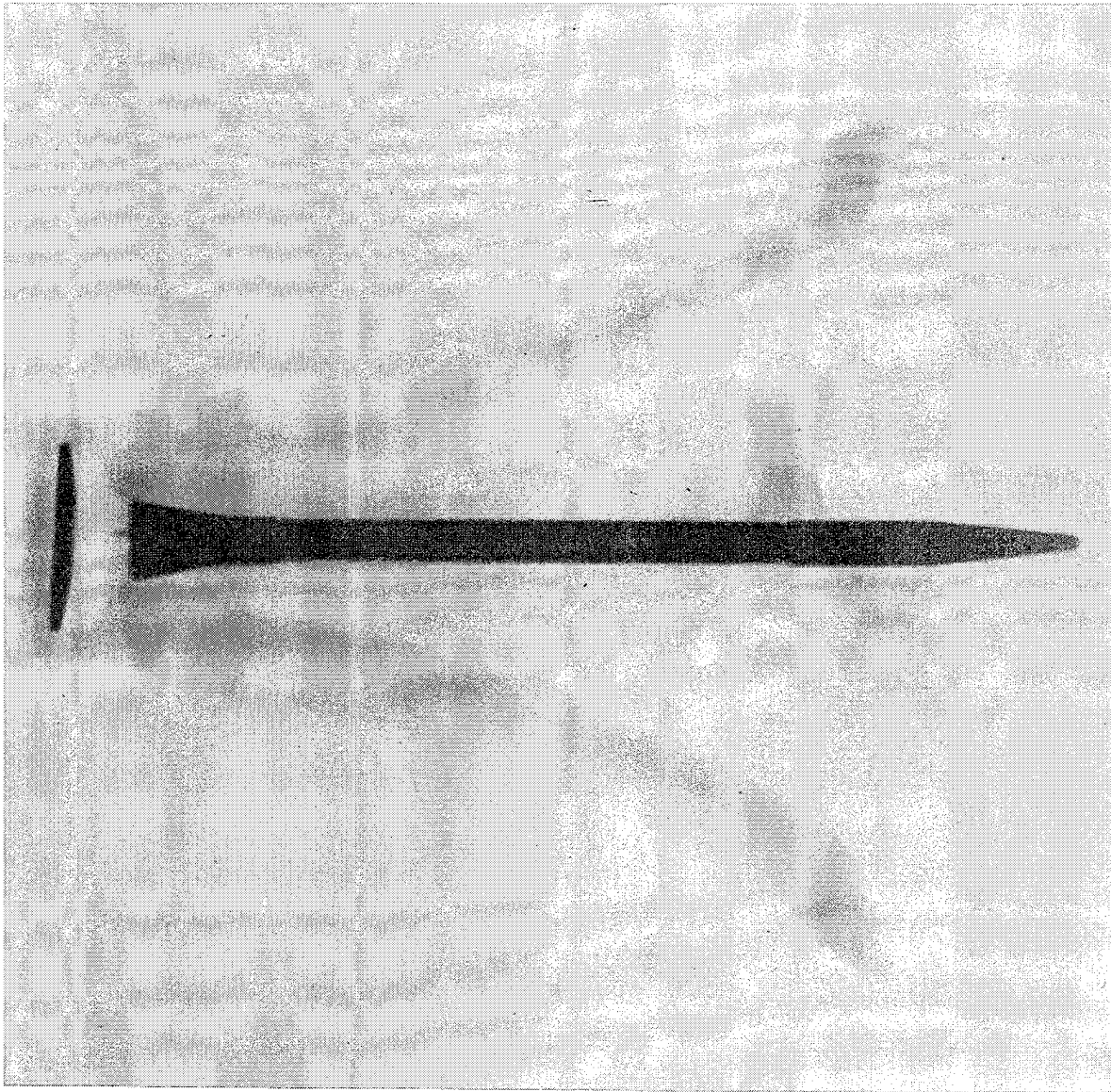(Mach = 5.3, 0.22 m from the gun muzzle)</u>.

Figure 5. X-ray of the sabot discard and structural integrity
(Mach = 5.3, 0.85 m from the gun muzzle).

Figure 6. Schematic of the aerodynamics range test setup.

projectiles. Use of the x-ray technique is discussed in Plostins et al. (1989), Plostins, Bornstein, and Celmins (1991), and Bornstein et al. (1992). The x-ray system is triggered by a piezoelectric gage that senses the precursor shock wave at the muzzle, then arms and waits for the main blast wave. The main blast wave arrives just after the projectile leaves the muzzle of the gun. This system is very reliable in obtaining x-ray images immediately after shot exit. During Phase I testing, only two of the x-rays were used and they were located 0.22 and 0.85 m downrange of the muzzle. The position of the two x-rays was shifted slightly between Phase I and Phase II because other testing had taken place. In Phase II, the x-ray positions were 0.19 and 0.70 m downrange of the muzzle.

A piezoelectric gage is used to record chamber pressure in the T-69 cannon. This is done to verify that the combustion process in the chamber is occurring as predicted, and it provides data to verify interior ballistic estimates should charge modification be required. The T-69 gun used for the test has a 37-mm chamber, necks down to 20-mm bore diameter, and has a barrel length of 3.048 m.

The range facility itself consists of 35 orthogonal spark shadowgraph stations arranged in five groups over 100 m of trajectory length. The first station is located approximately 4.57 m downrange of the muzzle. Infrared sensors detect the passage of the projectile, and a computer system triggers the spark sources that project on film a vertical and horizontal direct image of the passing projectile. This range facility is unique in that it is the only facility in the world that takes a direct image on film. All other ranges take a photograph of the shadow on a screen. The direct image technique allows the facility to produce high-quality spark shadowgraphs, but limits the size of the projectiles that can be tested. The stations are all surveyed into a fiducial system that is simultaneously imaged on the film with the projectile. Braun (1958) provides a detailed description of the Aerodynamics Range Facility.

The film is processed after each shot. The position and angle of the projectile are extracted from the images using a computerized digitizer system controlled by a personal computer. The data is transferred to a mainframe computer for analysis. The data reduction technique utilizes an inverse procedure. The range data provides the center-of-gravity location and the angular orientation of the projectile at discrete points along the trajectory. The data reduction procedures assume a model for the aerodynamic forces and moments and then use numerical procedures to infer the forces and moments that were required to produce the measured trajectory. Two different data reduction techniques were used for this program: a linear procedure developed at ARL and detailed in Murphy (1963), and a full 6 degree-of-freedom (DOF) procedure developed for the U.S. Air Force Wright Laboratories that is outlined in Hathaway and

8

Whyte (1979). The full 6-DOF procedure has the advantage that it can do multiple round reductions, identify spin yaw resonance, and extract nonlinear aerodynamic coefficients.

3. PHASE I TESTING DATA AND RESULTS

Six subscale, fluted, flare-stabilized penetrators were launched during Phase I testing. A schematic of the penetrator was presented earlier in Figure 2. The physicals for the flight body are given in Table 1. Half of these penetrators had two opposing flutes canted to provide roll control, while the other half had no cants. On the three penetrators with the cant, the last 2.54 mm of the two opposing flutes was beveled to 4°. The details of this are shown in Figure 2. All rounds were fitted with spin pins to measure the roll history of the projectile. The rounds with canted flutes are identified in the test matrix given in Table 2. Table 2 also gives the measured muzzle velocity, the launch weight of the penetrator/sabot assembly, the measured peak, chamber pressure, and the approximate trajectory distance over which range data was obtained. The average muzzle velocity was a little higher than the predicted 1,850 m/s. The charge was a mixture of 37-mm propellant and 25-mm propellant blended to achieve 1,850 m/s based on the calculations of Anderson and Fickie (1987). Since the grain and web sizes were very different, it was a little difficult to precisely control the combustion process, and consequently, the muzzle velocity. The average muzzle velocity was 1,868.5 m/s with a standard deviation of 9.6 m/s. Some of the rounds flew to the fifth group of range shadowgraph stations, a distance of about 85 m. However, the data in that group was lost because the rounds impacted on armor plate. Such impacts cause a flash and loss of the photographic data within a certain proximity of the impact. The column in Table 2 labeled "Approximate Distance" gives the maximum distance over which good range data was recorded.

The linear data-reduction method described in Murphy (1963) is used to initialize the 6-DOF data reduction. A complete example of a data fit of round no. 20448 using the 6-DOF technique of Hathaway and Whyte (1979) is provided in Figures 7–13. Figures 7 and 8 show the horizontal and vertical center of gravity trajectory data and the analytical fit. Figure 9 gives yaw (β) and pitch (α). Figure 10 is a plot of total angle of attack (δ) as a function of range. Clearly this plot and Figure 11 (pitch vs. yaw) show the total angle of attack is increasing as the penetrator proceeds downrange. Figure 12 plots the roll data and the fit to the roll data obtained. Figure 13 provides the roll rate extracted from the roll data as well as an indication of the fast arm yaw frequency. It is interesting that round no. 20448 had no fin cant, yet

9

Table 1. Phase I and Phase II Penetrator Physical Parameters

QUANTITY	PHASE I FLUTED FLARE	PHASE II FLUTED FLARE	PHASE II FIN
DIAMETER (m)	0.005	0.005	0.005
MASS (kg)	0.01376	0.01435	0.01445
Ix (kg–m²)	0.423×10^{-7}	0.408×10^{-7}	0.437×10^{-7}
Iy (kg–m²)	0.119×10^{-4}	0.133×10^{-4}	0.135×10^{-4}
CG (m from Base)	0.0458	0.0558	0.0557
L/D	20.756	22.84	22.84

Table 2. Phase I Test Matrix and Preliminary Results

ARL ROUND #	CANT	VELOCITY (m/s)	LAUNCH WEIGHT (grams)	CHAMBER PRESSURE (MPa)	APPROX. DISTANCE (m)
20443	YES	1877	55.97	373	46
20444	NO	1874	55.00	398	85
20445	NO	1871	55.51	407	5
20446	YES	1873	55.11	401	85
20447	YES	1848	55.41	387	85
20448	NO	1868	55.21	391	64
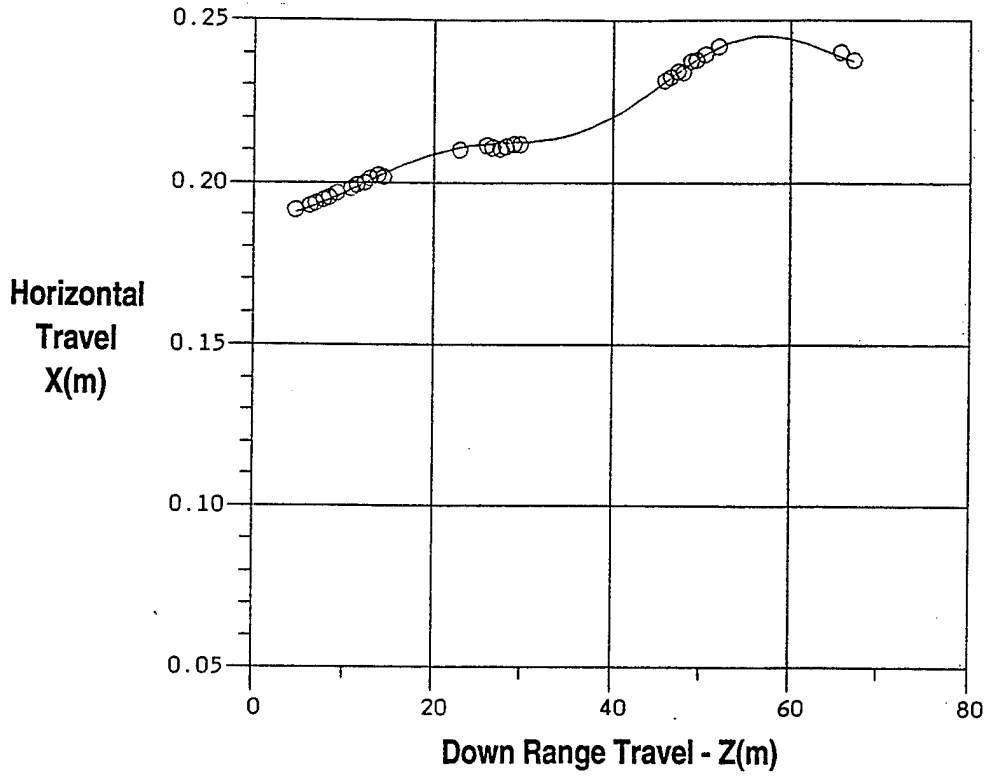
Figure 7. Horizontal center-of-gravity trajectory fit (round no. 20448).
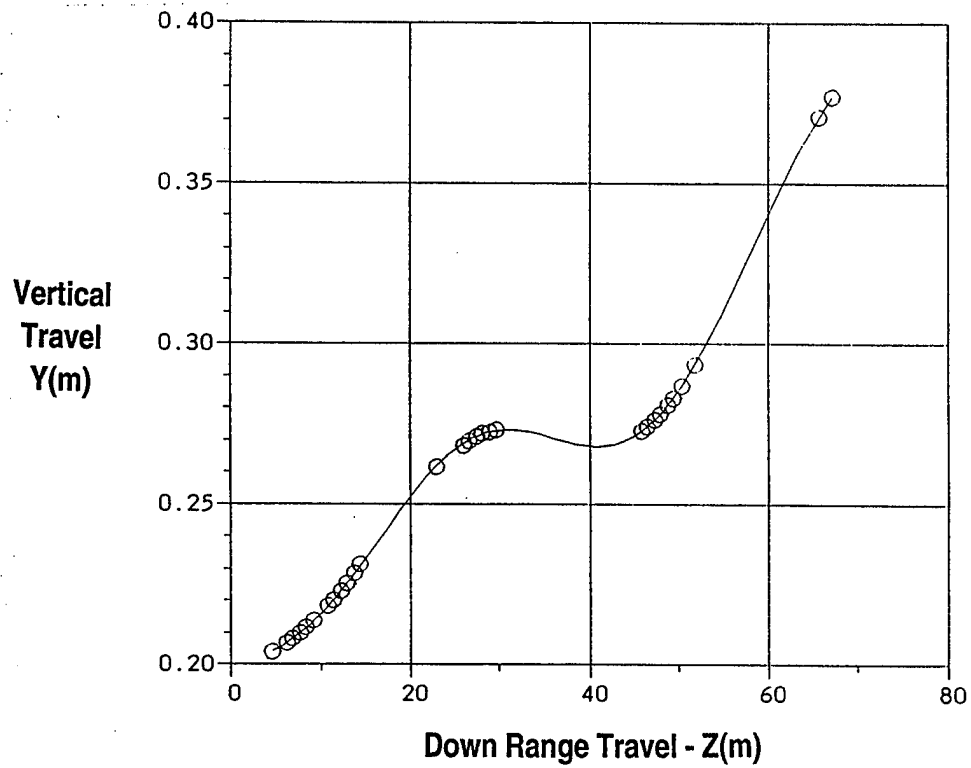
Figure 8. Vertical center-of-gravity trajectory fit (round no. 20448).

11
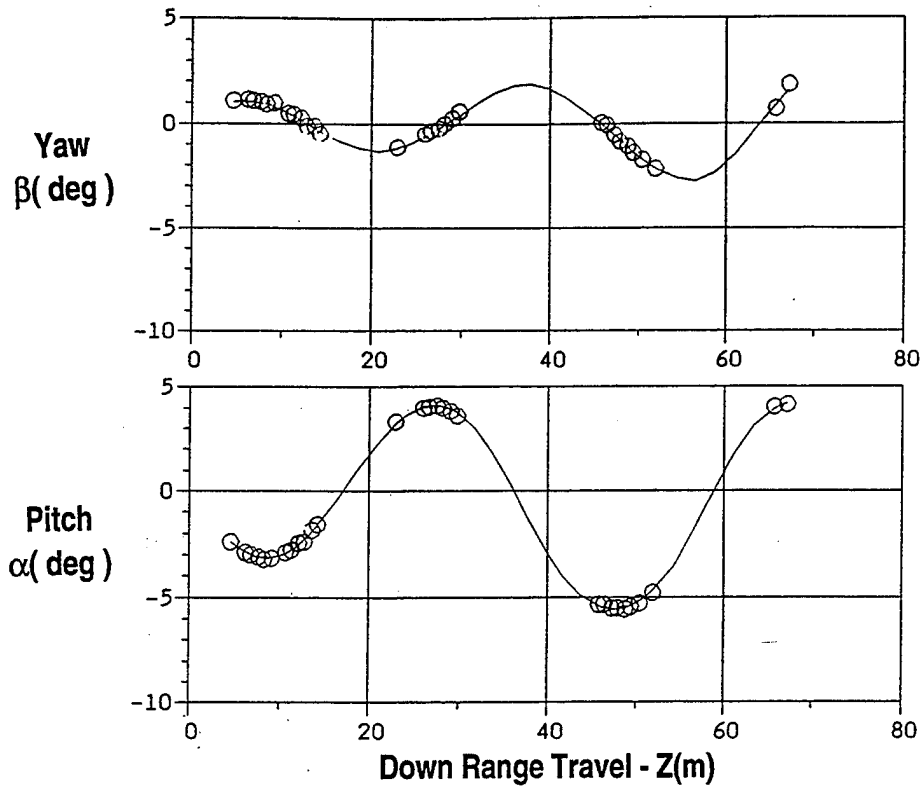
Figure 9. Angular trajectory motion fit; yaw and pitch (round no. 20448).
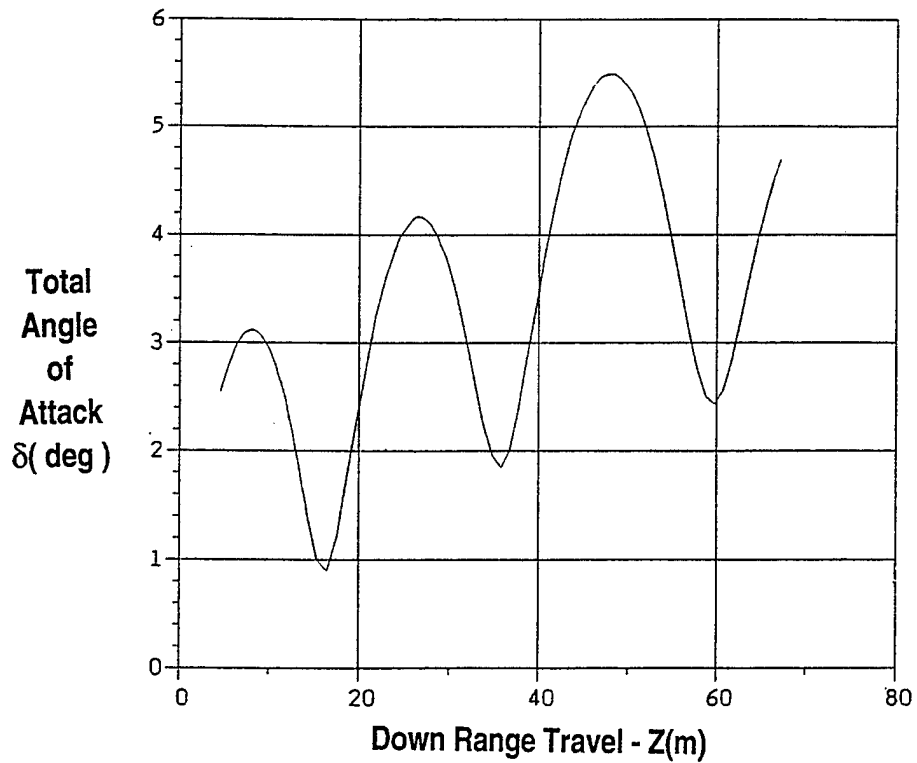
Figure 10. Total angle of attack vs. range (round no. 20448).
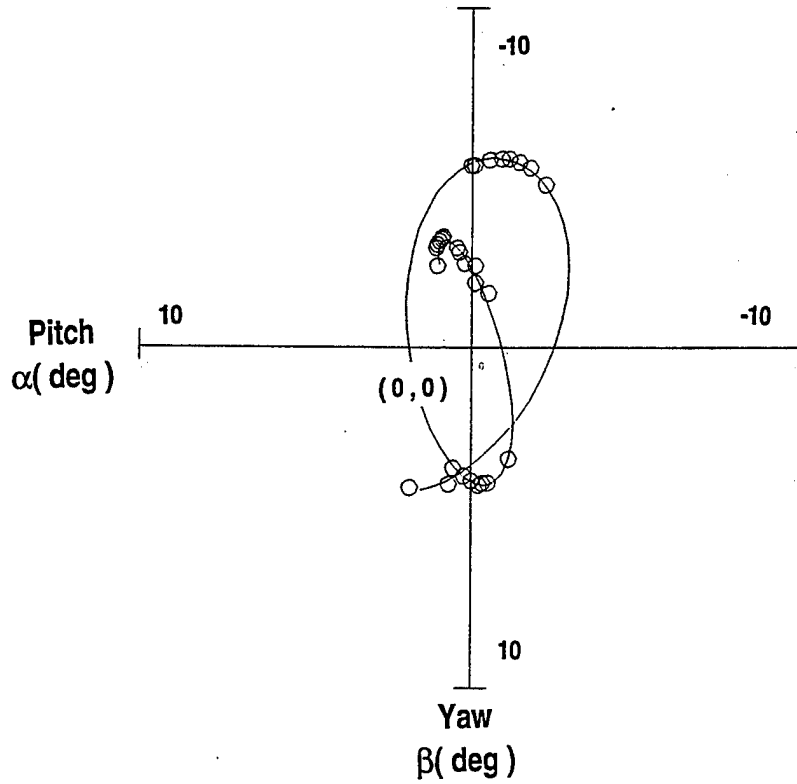
Figure 11. Pitch vs. yaw (round no. 20448).
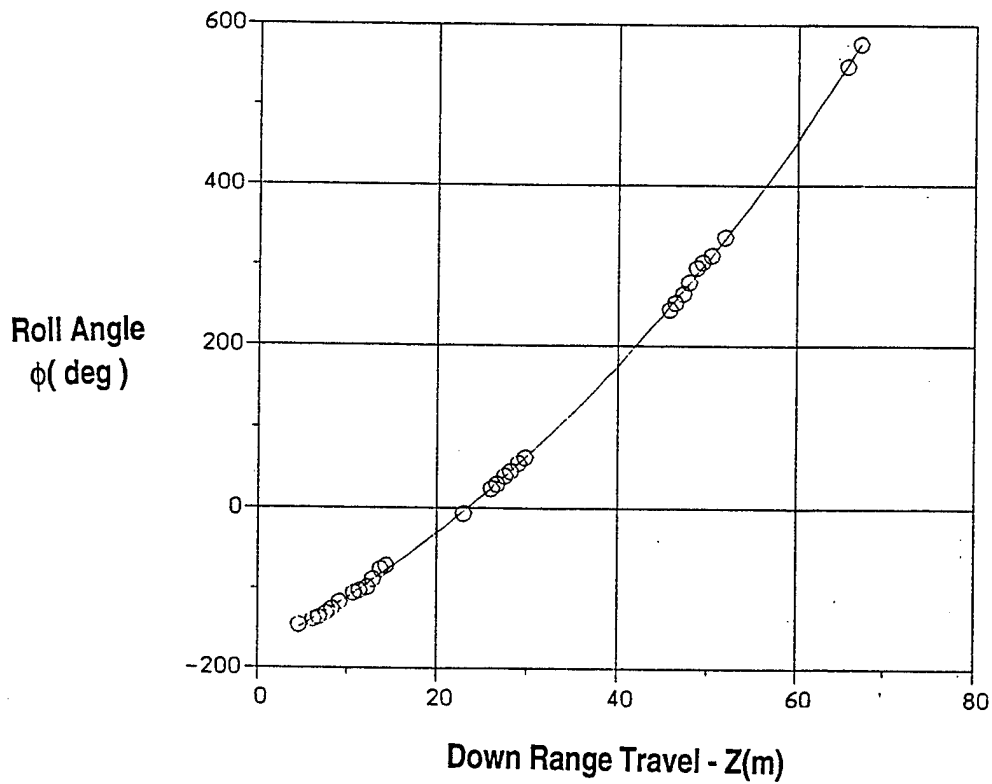
Figure 12. Vehicle roll angle vs. range (round no. 20448).

13
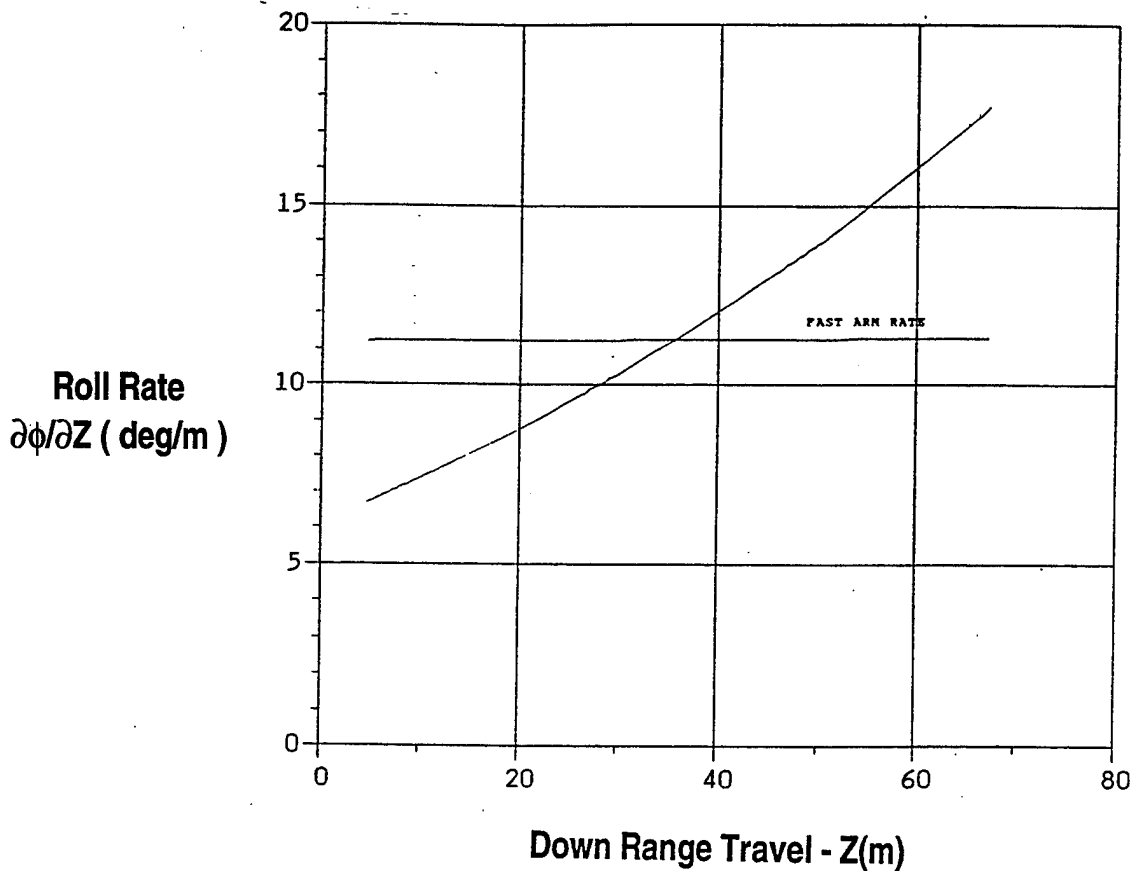
Figure 13.   Vehicle roll rate vs. range (round no. 20448).

clearly the projectile is rolling up along its trajectory. Note the projectile is going through roll-yaw resonance at approximately 35 m. This data is typical of the data obtained on most of the rounds.

Figure 14 is a plot of the roll histories for all six penetrators. The roll behavior of these penetrators is interesting. The available data indicates that uncanted penetrators roll up and the roll rate does not appear to be significantly higher for projectiles with beveled flutes. Round no. 20447 is an exception because its roll rate increased at a faster rate. Round no. 20447 is discussed in detail later in this section. One possible explanation is that the penetrators were threaded rather than grooved and the subscale penetrators were inadvertently fabricated with the full-scale thread depth. The full-scale depth of the threads was approximately 0.5 mm. This reduced the already small roll moment of inertia of the subscale penetrator relative to that of the full-scale penetrator. From shadowgraphs obtained (Figures 15a and 15b), it is clear the boundary layer is turbulent and grows quite thick over the region of the threads. This creates a region of low-energy flow that extends some distance from the surface. The flare is largely immersed in this low-energy flow. Under these circumstances, the effectiveness of the beveled flutes as roll-generating surfaces is questionable. Roll torque generated by the flow over the threads could have

14
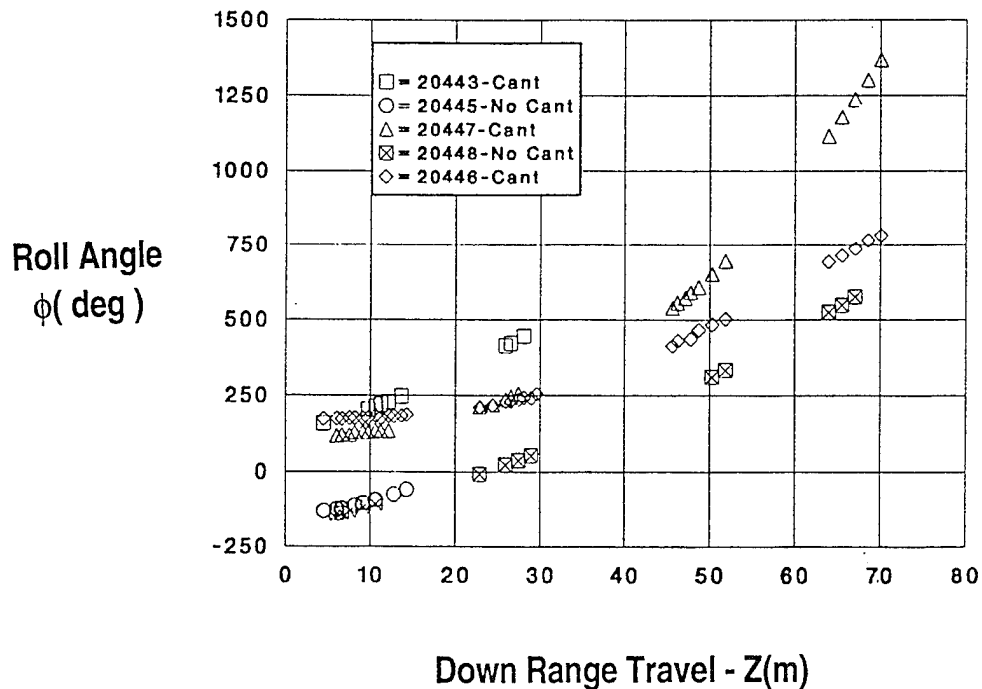
Figure 14. Vehicle roll summary.

overwhelmed that produced by the right-hand flutes. The threads were right handed, and they would tend to produce a right-hand roll.

Three rounds, nos. 20443, 20446, and 20448, were chosen to do a multiple round reduction. This was possible because a roll history had been obtained for each over a good portion of the trajectory. The results of this analysis are presented in Table 3. The error estimates in the final column of Table 3 are measures of the ability of the 6-DOF fitting technique to fit the data to the aerodynamic model. An approximate one sigma standard deviation on the coefficient can be obtained from the following relationship:

$$\pm\sigma = \pm\% \text{ Error} \times \text{Aerodynamic Coefficient}$$

The estimates do not account for the measurement error in the position and angle data itself. There was some difficulty in obtaining converged fits. It was only possible to come to a converged solution if each round was allowed to have its own unique roll torque. This is reflected in the table by the three unique trim angles and roll torque coefficients. Also it was not possible to fit the data concurrently without allowing for a nonlinear static-moment coefficient.

15
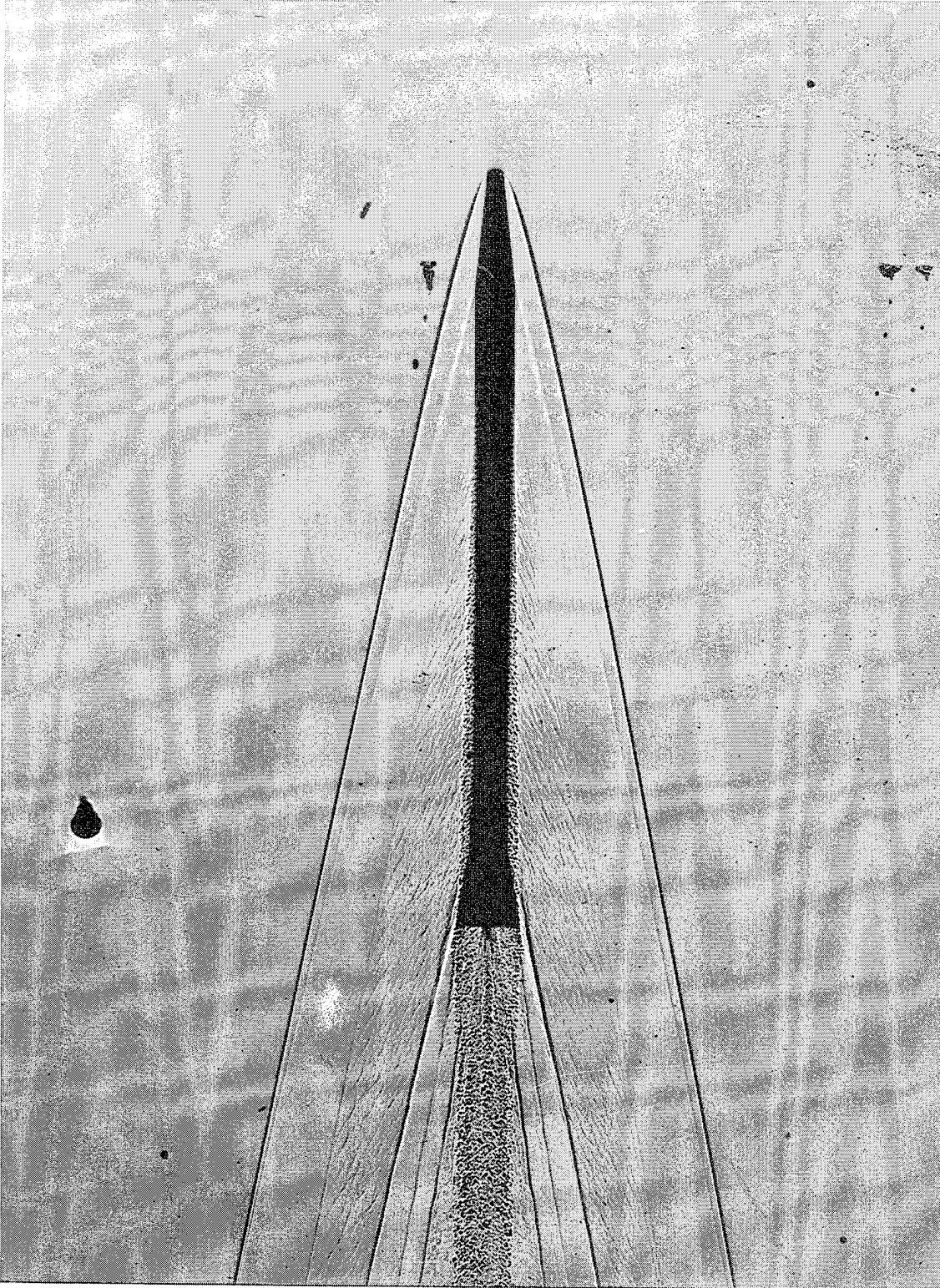
Figure 15a. <u>Free-flight shadowgraph of the fluted, flare-stabilized penetrator ($\beta = 0°$) (Mach no. = 5.49) (round no. 20448).</u>
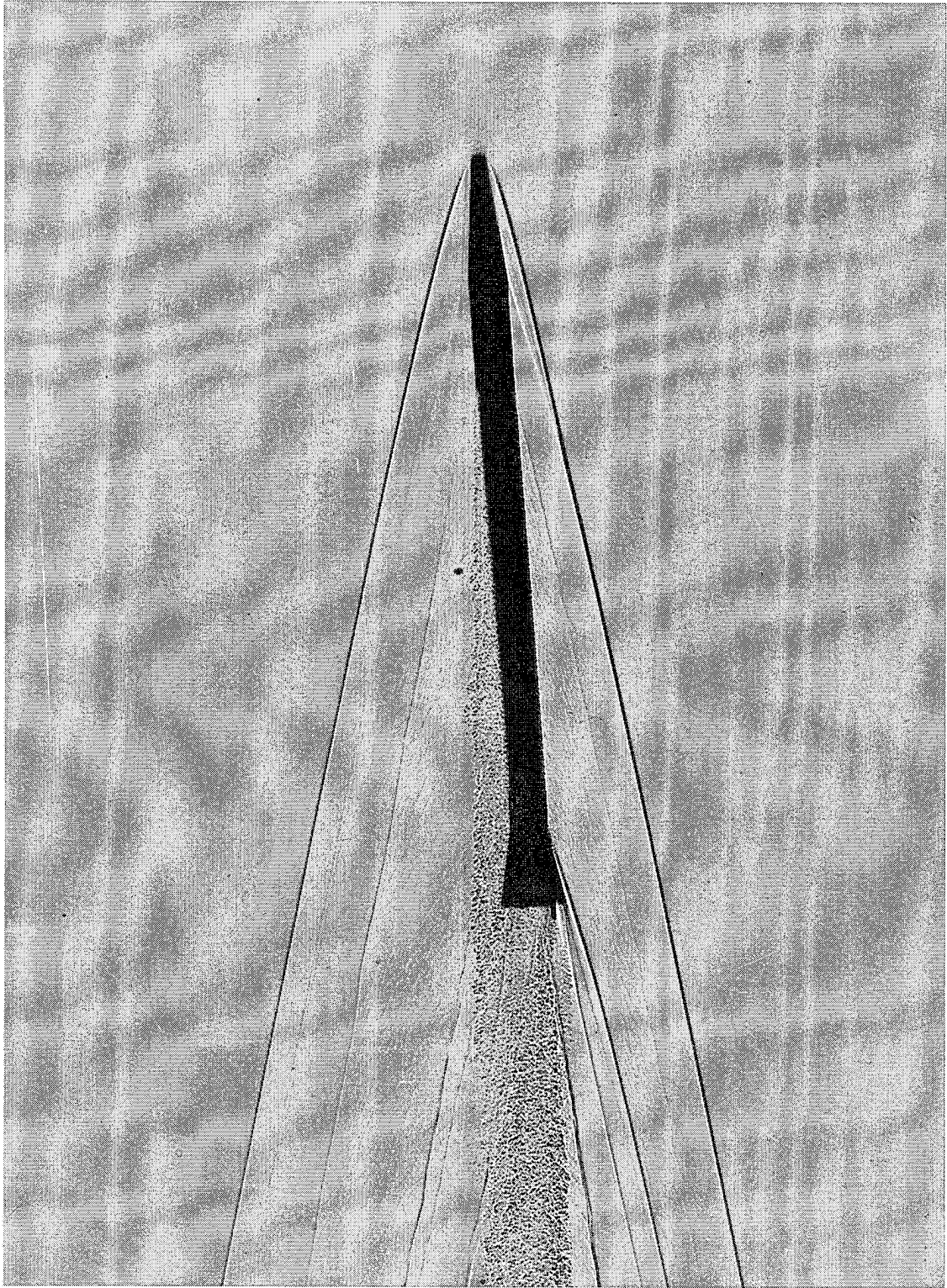
Figure 15b. Free-flight shadowgraph of the fluted, flare-stabilized penetrator ($\beta = 5.37°$) (Mach no. = 5.44) (round no. 20447).

Table 3. Phase I Multiple Round Data Fit Results

COEFFICIENT	SYMBOL	VALUE	ERROR (%)
AXIAL FORCE	C_x	0.42	1.43
YAW DRAG	$C_{x_\alpha}{}^2$	5.64	20.0
NORMAL FORCE	C_{N_α}	6.39	1.2
STATIC MOMENT	C_{m_α}	−10.77	0.78
CUBIC STATIC MOMENT	$C_{m_\alpha}{}^3$	1702.3	0.95
QUINTIC STATIC MOMENT	$C_{m_\alpha}{}^5$	-99.25×10^3	*
PITCH DAMPING MOMEMT	$C_{m_q} + C_{m_\alpha}$	188.5	19.0
ROLL DAMPING MOMENT (pd/2V SYSTEM)	C_{l_p}	−1.63	16.87
ROLL TORQUE MOMENT (#20443)	C_{l_δ}	0.00653	10.1
ROLL TORQUE MOMENT (#20446)	C_{l_δ}	0.00502	4.6
ROLL TORQUE MOMENT (#20448)	C_{l_δ}	0.00383	7.3
TRIM ANGLE (#20443)	α_0	0.54	1.63
TRIM ANGLE (#20446)	α_0	0.65	4.5
TRIM ANGLE (#20448)	α_0	0.31	2.0
STATIC MARGIN (ZERO YAW)	ΔX_{op}	8.1 (%)	*

NOTE: 6 DOF REDUCTION

The static-moment coefficient was fit up to a quintic term. The total static moment coefficient, C_m, was plotted against angle of attack. Two curves are shown in Figure 16, one truncated at α^3 and the second at α^5. These two curves represent two possible solutions for C_m. The actual curve for the total static moment is probably somewhere in the shaded region. This leads to an interesting conclusion: it is possible for this round to go unstable at angles in excess of 6°. Round no. 20447 provided experimental evidence to support this conclusion. Figure 17 is a plot of yaw (β) and pitch (α). Round no. 20447 appears to begin a yaw cycle and then diverges. This is clearer in Figure 18, the plot of total angle of attack vs. range; at 30 m the total angle of attack increases without bound. Comparing the data for round no. 20447 (Figure 18) with that for round no. 20448 (Figure 10), both rounds exhibit increasing total angle

18

The figure shows a plot of Total Static Moment Coefficient C_m (y-axis, from -1.0 to 0.0) versus Total Angle of Attack (deg.) (x-axis, from 0 to 12).

$$C_m = C_{m_\alpha}\alpha + C_{m_{\alpha^3}}\alpha^3$$

EXTRAPOLATION

6 DOF FIT

$$C_m = C_{m_\alpha}\alpha + C_{m_{\alpha^3}}\alpha^3 + C_{m_{\alpha^5}}\alpha^5$$

EXTRAPOLATION

$C_{m_\alpha} = -10.77$

$C_{m_{\alpha^3}} = +1702.3$

$C_{m_{\alpha^5}} = -99.25 \times 10^3$
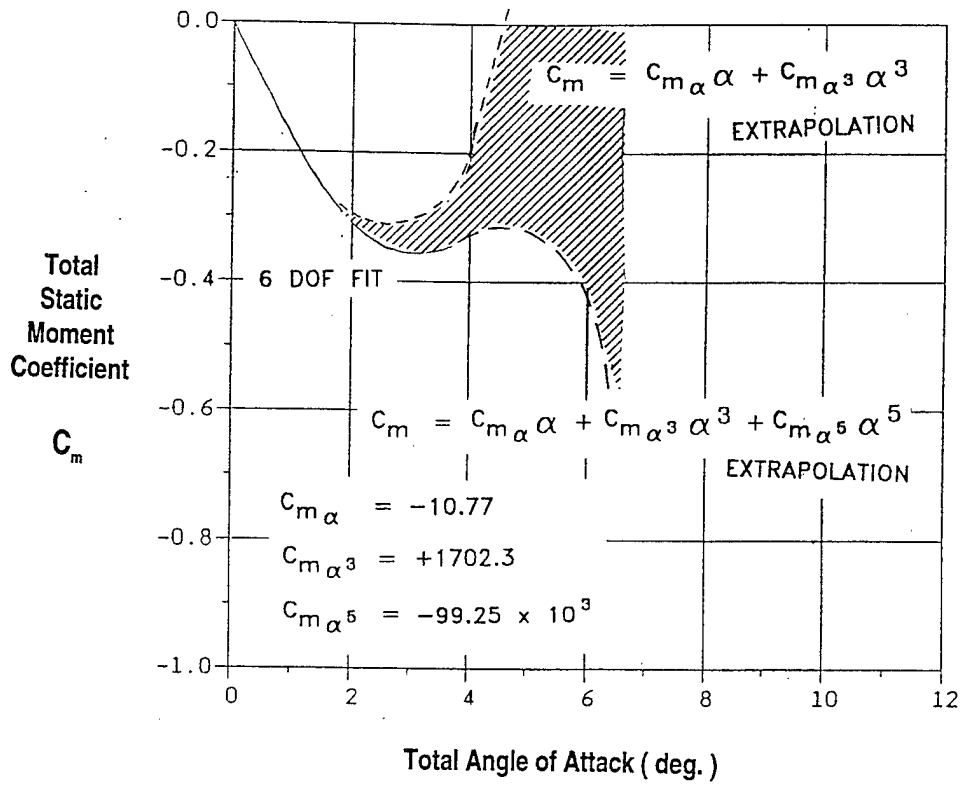
Figure 16. Total nonlinear static moment coefficient vs. total angle of attack.
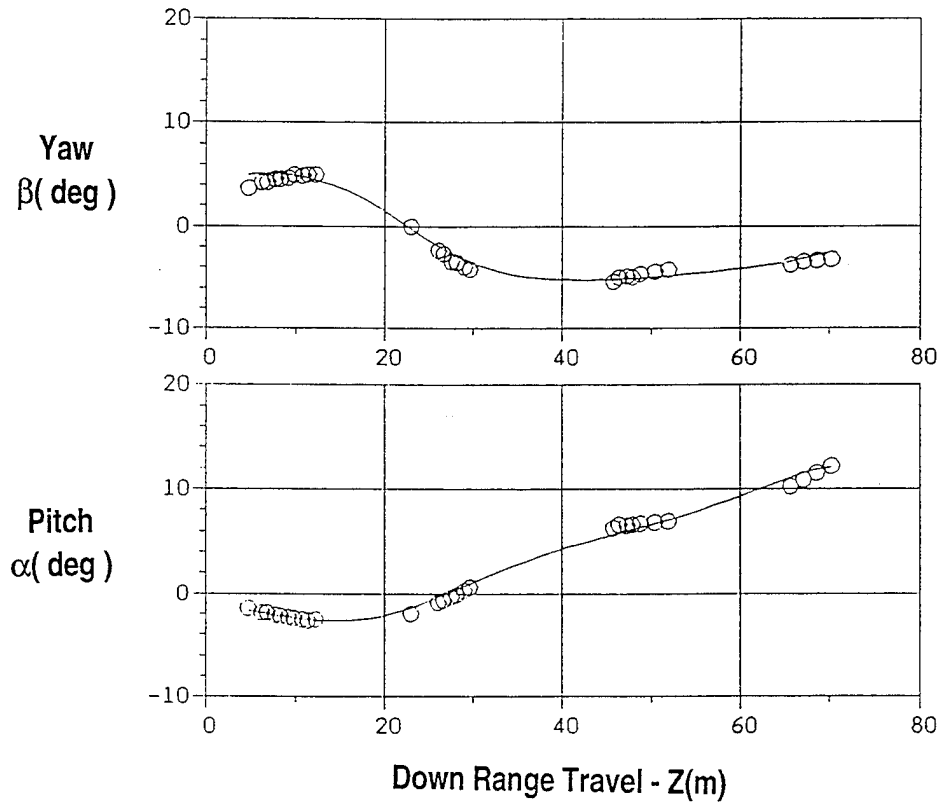
Figure 17. Angular trajectory motion fit; yaw and pitch (round no. 20447).

19
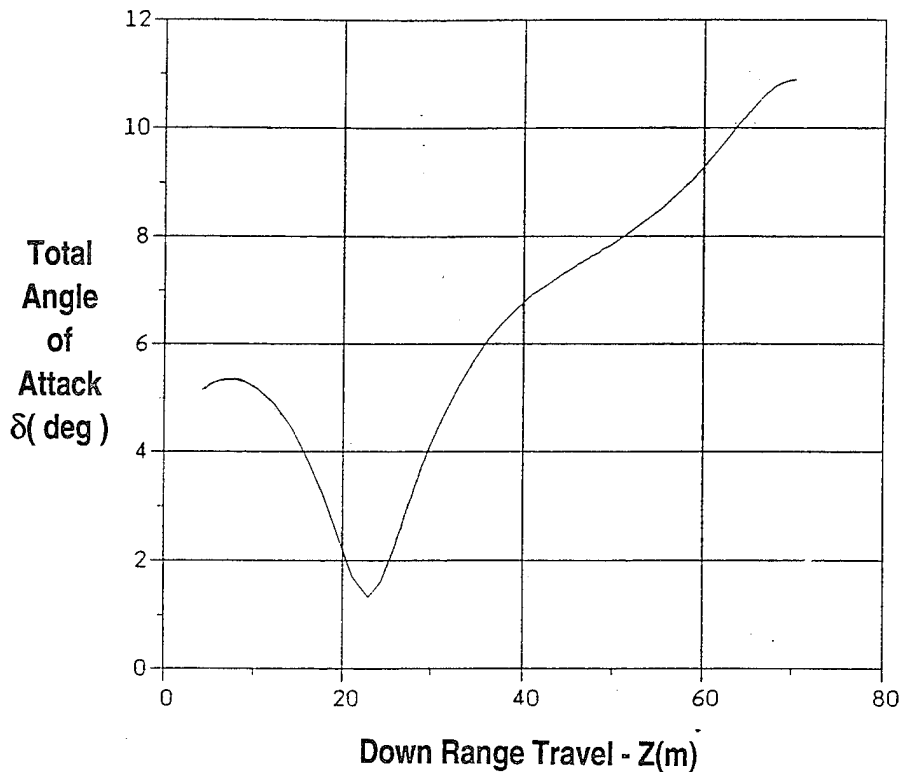
Figure 18. Total angle of attack vs. range (round no. 20447).

of attack vs. range. Round no. 20448 has a lower first maximum angle of attack. Round no. 20447 probably demonstrated unstable behavior early in the flight due to higher launch yaw rates. Figure 19 shows that at 22 m, round no. 20447 is at roll yaw resonance. At this condition the yaw is expected to grow, but eventually a well-behaved round will drive that yaw back down as the roll increases beyond the yaw frequency. At angle of attack, a larger portion of the fluted flare is immersed in the free stream as shown in Figure 15b. The high pressure on the windward side increases the stabilizing effect of the flare. It is postulated that, despite this, the fluted flare is still too small. Above an angle of attack of 6° the nose lift outweighs the ability of the fluted flare to stabilize the projectile. The static margin at zero angle of attack is approximately 8.1%, but because of the nonlinear static-moment coefficient and constant lift coefficient, it rapidly diminishes with increasing angle of attack.

No fits could be obtained that produced a negative pitch-damping moment coefficient. Physical insight would dictate that the coefficient be negative since this is a damping phenomenon. All of the rounds that were tested passed through roll yaw resonance within the confines of the range trajectory. To

20
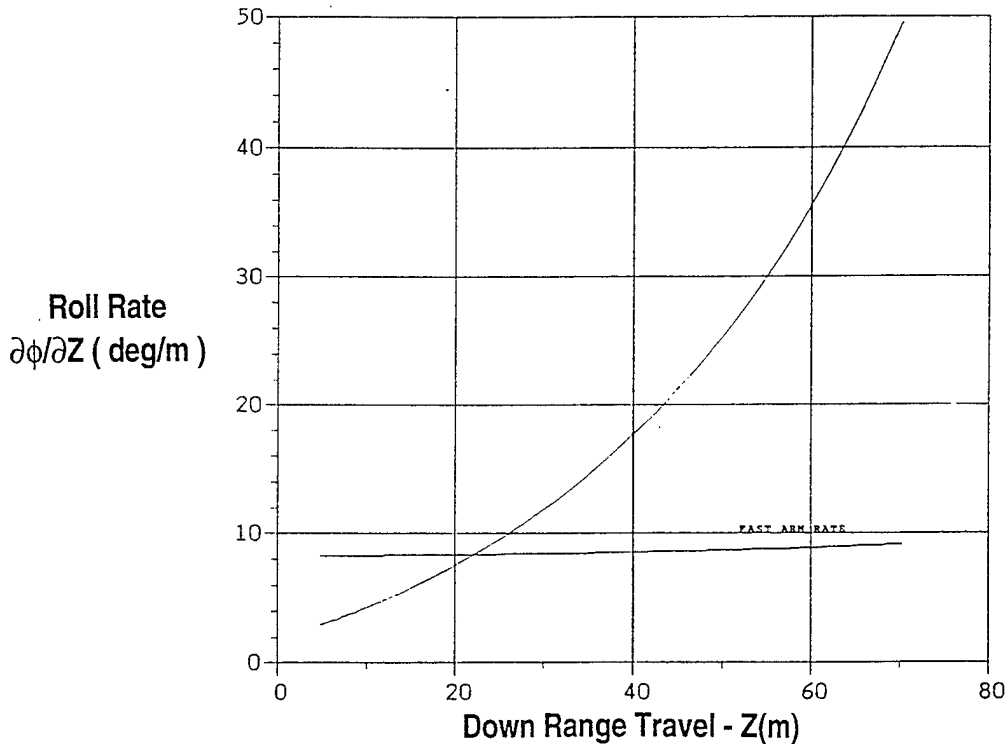
Figure 19. Vehicle roll rate vs. range (round no. 20447).

determine a good number for the pitch-damping coefficient, it is generally necessary to have five half cycles of decaying yaw. None of the rounds tested had more than three half cycles of yaw data, so the pitch-damping coefficient reported in Table 3 is suspect based on the analysis, insufficient data, and physical insight. The coefficient is reported for consistency and completeness of the data fit output, but is not a measure of the pitch damping of this penetrator. This concludes the discussion of Phase I testing results.

4. REDESIGN CONSIDERATIONS

The goal of the CCEMG program was to optimize the performance and mitigate risk of the full-scale designs through subscale tests. Two full-scale designs were proposed by KSC as a result of Phase I testing. These designs are shown in Figures 20a and 20b. Both designs have buttress grooves rather than threads, and both have smaller nose radii to reduce drag. The first configuration uses the same fluted flare as the previous design as shown in Figure 1. The flare was moved back on the penetrator to improve static margin. The second design uses a cruciform tail. Both full-scale penetrators are made of tungsten

21
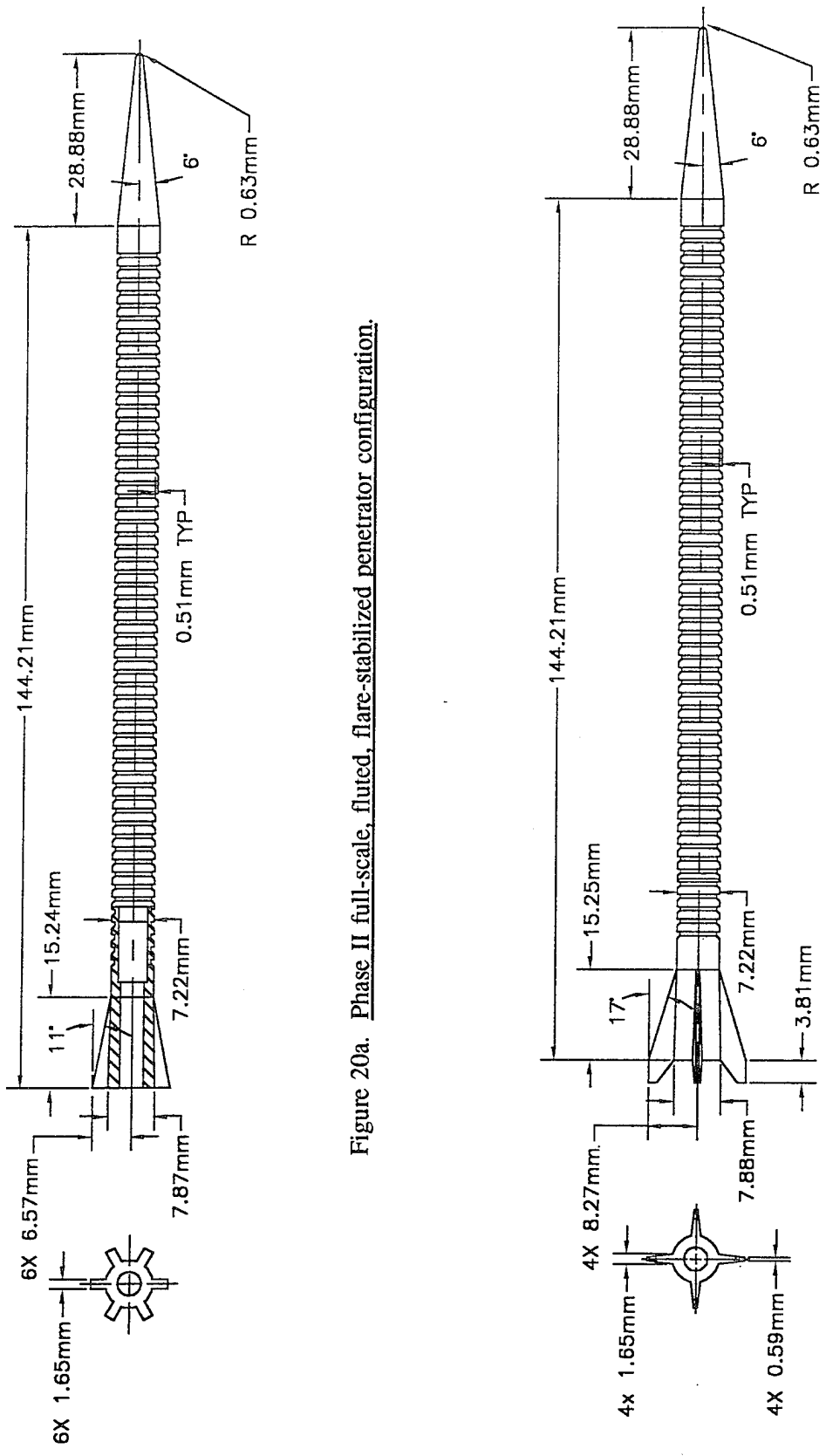
Figure 20a. Phase II full-scale, fluted, flare-stabilized penetrator configuration.

Figure 20b. Phase II full-scale, cruciform, fin-stabilized penetrator configuration.

22

alloy (x27x) with screw-on titanium afterabodies. The changes in the full-scale designs were integrated into the Phase II subscale penetrators.

The subscale penetrators tested in Phase II are shown in Figures 21a and 21b. To improve the drag, the threads were changed to buttress grooves that had a depth of only 7% of the body diameter, unlike the Phase I subscale penetrator, which had a thread depth of 10% of the body diameter. The threads were changed to grooves to eliminate any roll control problems they may have caused. Unlike the threads, the grooves have no twist, so the new Phase II configuration ensured that the beveled flutes provided the only roll control. Note in Figure 21a, the pitch per unit length of the grooves for the Phase II fluted flare penetrator is significantly less than the pitch of the threads for the Phase I penetrator (see Figure 2). It was hoped that the reduction in depth of the grooves and the lower pitch per unit length would reduce the growth of the boundary layer. A thinner boundary layer would shadow less of the fluted flare and improve the penetrator stability.

Due to structural concerns the Phase I penetrator was manufactured out of a monoblock of maraging steel. To improve the static margin and more closely approximate the mass distribution of the full-scale penetrators, the fluted flare-tail section was manufactured from aluminum. The aluminum was hard coated, half in, half out, in order to survive the in-bore thermal loads. A section of the maraging steel penetrator extended completely through the center of the aluminum fluted-flare fin assembly to the base of the projectile. The details of the design are shown in Figure 21. The maraging steel core provided the acceleration load structure for the sabot pusher to act on. Given these changes and the reduction in peak acceleration achieved during Phase I testing, the aluminum and steel aft end of the penetrator could now survive launch in the base-pushed configuration. The nose radius of the round was to remain the same at 0.035 in (0.889 mm) and not scaled so it could more readily be compared with the Phase I results. The nose radius was determined to be 0.040 in (1.02 mm) upon final inspection.

5. PHASE II TESTING DATA AND RESULTS

For Phase II, the general test setup, procedure, and data analysis were the same as for Phase I. Again, quality launches were achieved at Mach 5.5 as shown in Figure 22. Also good in-flight shadowgraphs of both configurations were obtained. These are shown in Figures 23 and 24. Table 1 provides the physicals on both flight bodies and Table 4 the test matrix for Phase II.
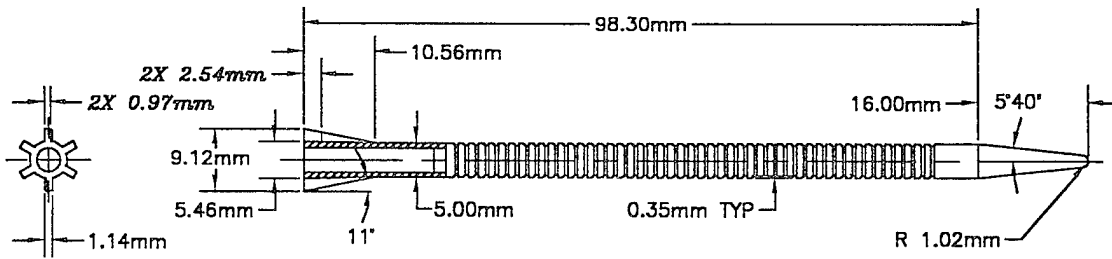
Dimensions in italics
define 4 degree roll cants

Figure 21a. Phase II subscale, fluted, flare-stabilized penetrator configuration.
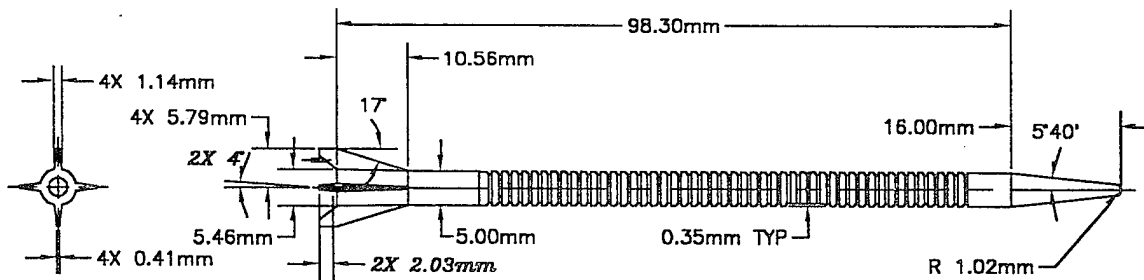
Dimensions in italics
define 4 degree roll cants

Figure 21b. Phase II subscale, cruciform, fin-stabilized penetrator configuration.

24
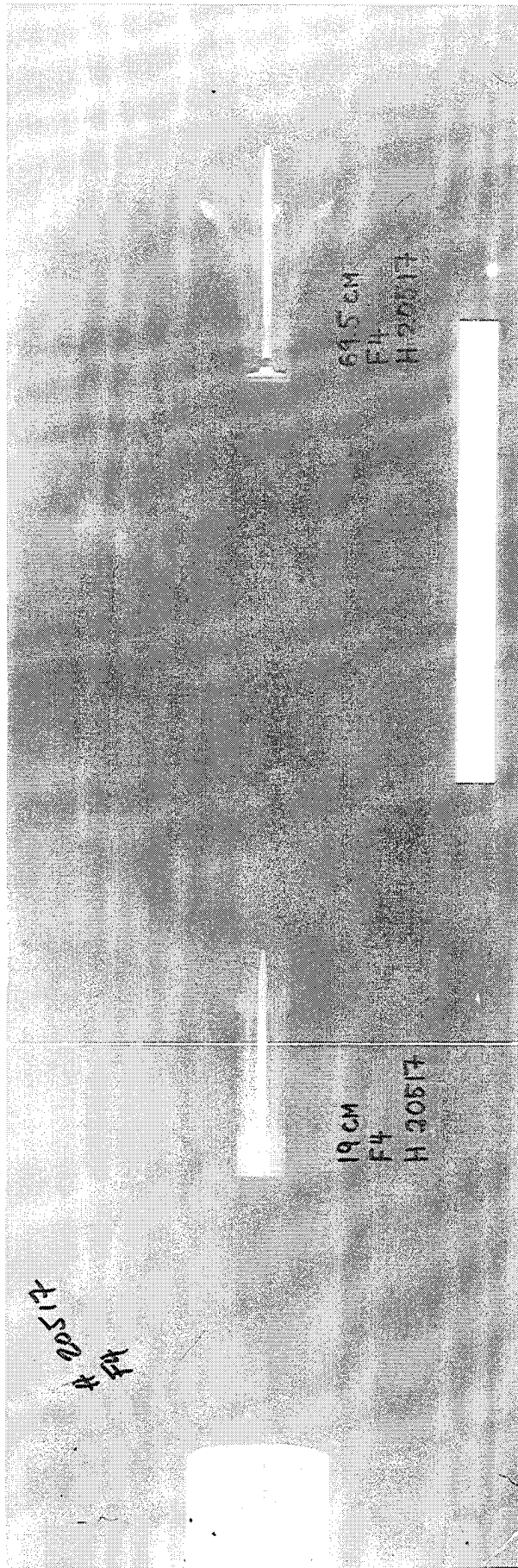
Figure 22. X-ray of the sabot discard and launch of the fin-stabilized penetrator.
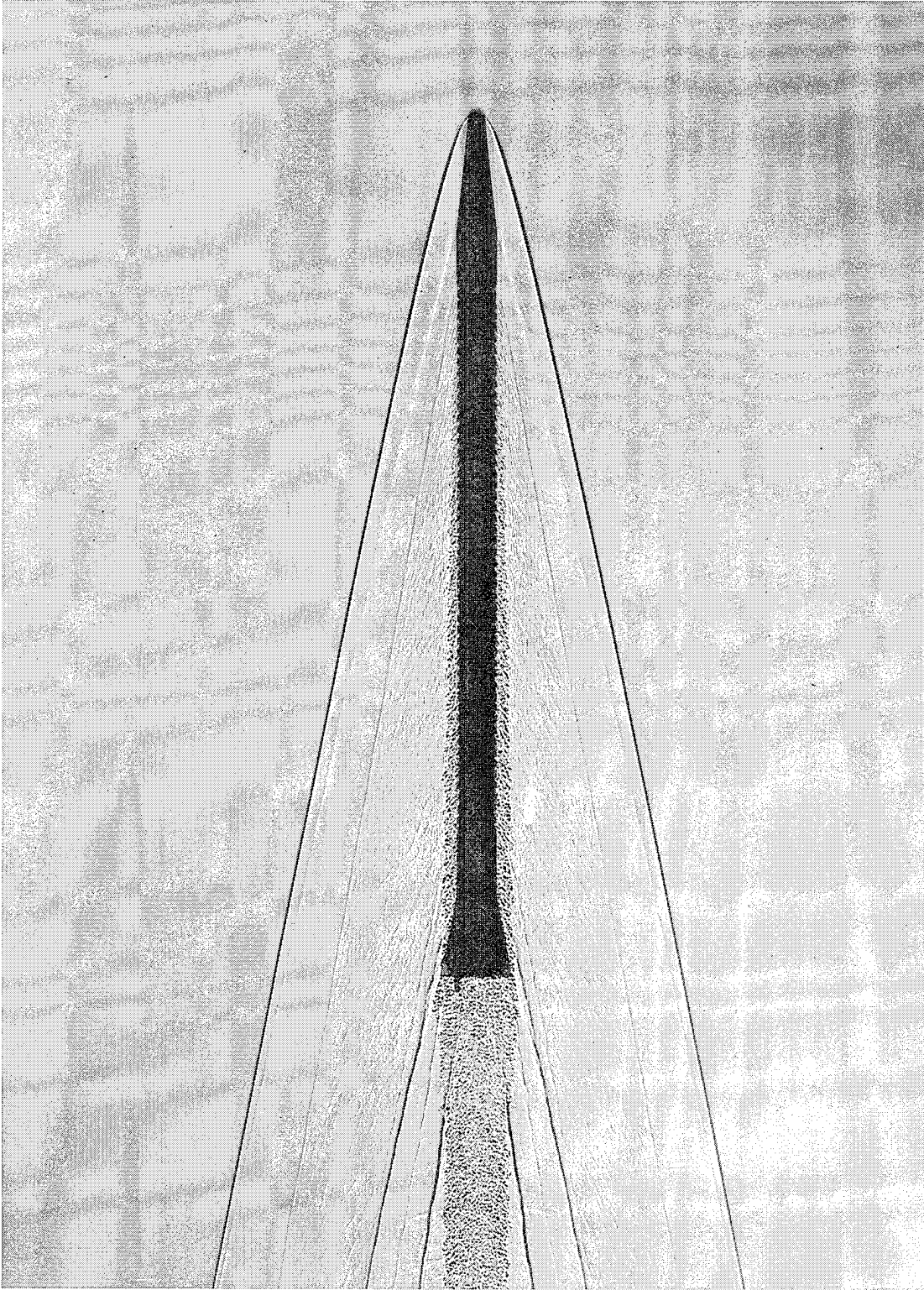
Figure 23. Free-flight shadowgraph of the Phase II fluted, flare-stabilized penetrator ($\alpha = 0°$) (Mach no. = 5.49) (round no. 20511).
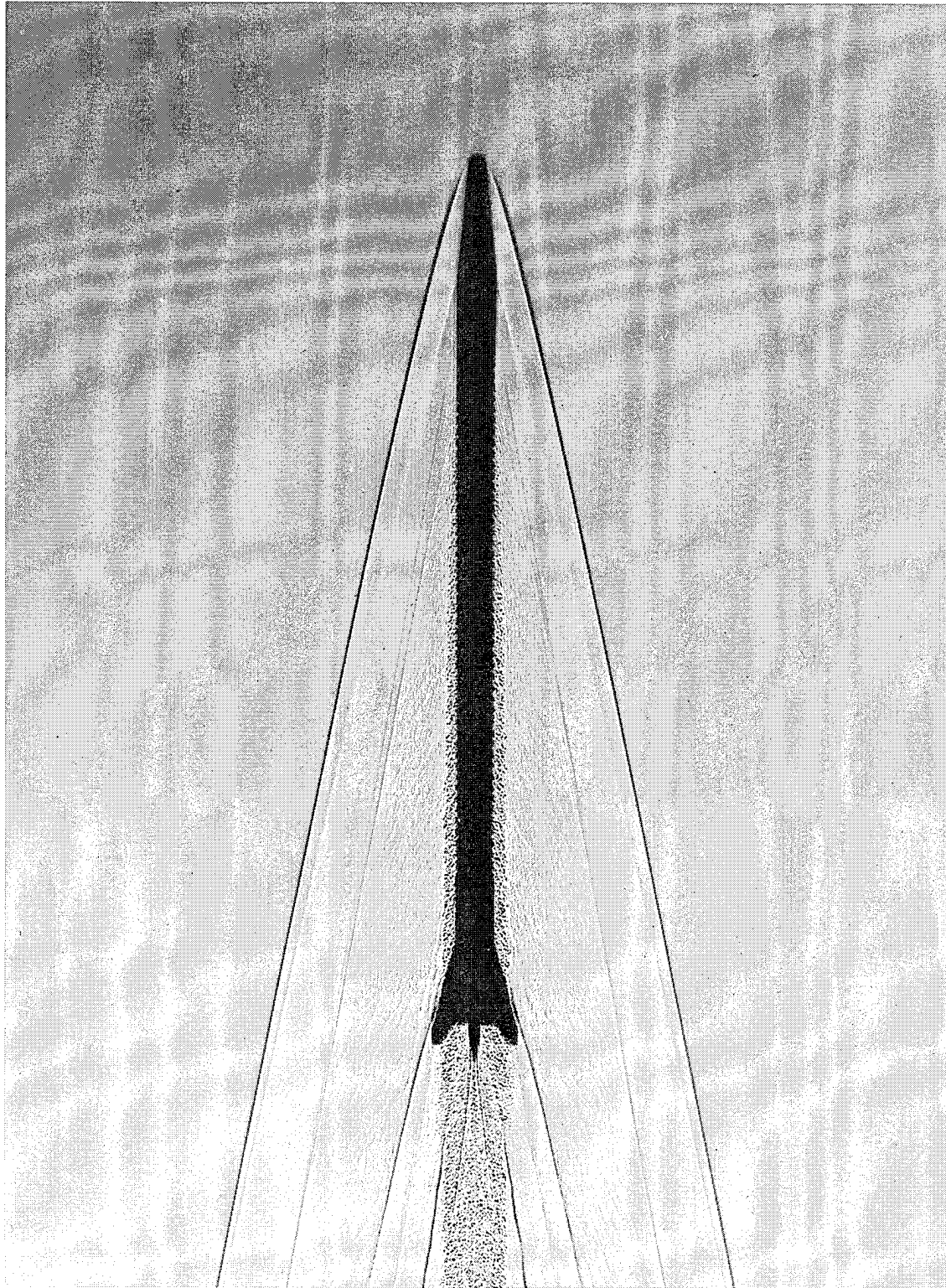
Figure 24. <u>Free-flight shadowgraph of the Phase II cruciform fin-stabilized penetrator ($\alpha = 0°$) (Mach no. = 5.49) (round no. 20514).</u>

Table 4. Phase II Test Matrix and Preliminary Results

ARL ROUND #	CANT	VELOCITY (m/s)	LAUNCH WEIGHT (grams)	CHAMBER PRESSURE (MPa)	APPROX. DISTANCE (m)
20510	YES	1962	56.35	408	85
20511	YES	1866	57.70	385	85
20512	YES	1923	55.99	404	85
20513	YES	1876	55.73	378	85
20514	YES	1867	57.02	368	85
20515	YES	1878	56.66	408	85
20516	YES	1856	57.07	307	85
20517	YES	1874	57.27	373	85

20510-20513 (Fluted Flare) 20514-20517 (Fin)

Diagnostics for assessing roll proved difficult during this phase. The roll pin at the base of the projectile had problems separating from the sabot pusher. Of the eight rounds fired, five of the rounds had the roll pins pulled out during the launch. Only three data rounds with a full roll history were obtained. Thus, a 6-DOF reduction could only be done on these three rounds. Complete roll data was obtained on one fluted, flare-tail round (no. 20511), and two fin-stabilized rounds (nos. 20514 and 20515).

Table 5 lists the results of the 6-DOF fit of round no. 20511. The changes to the design resulted in some improvements. The drag was reduced significantly, the static moment coefficient increased, the lift appeared to have increased, and the static margin was slightly larger. Since the Phase II penetrator is longer and has a larger nose radius, it appears changing from threads to reduced depth grooves improved the overall drag. The fit error in determining the lift for this round is about 25%, so the lift coefficient can be anywhere from 6.21 to 10.28. The reason for this is that yaw is low (see Figure 25), and consequently, the swerve radius is small. The swerve radius was on the order of one millimeter. It is only possible to read the range film to 0.5 mm, making it difficult to measure the swerve trajectory and extract a well-determined lift coefficient. The lift coefficient for the Phase I penetrator is approximately 6.4, and the lift coefficient was extracted from a multiple fit. The confidence level in this number is much higher. The aerodynamic shape of the Phase II fluted flare configuration relative to the Phase I configuration is only different in two aspects: (1) it has grooves, and (2) it is slightly longer at L/D = 22.8. Since the Phase II penetrator is longer, the lift should increase. Therefore, the 8.28 number in Table 5 appears reasonable given the available data.

Table 5. Data Fit Results Round No. 20511

COEFFICIENT	SYMBOL	VALUE	ERROR (%)
AXIAL FORCE	C_x	0.35	0.2
YAW DRAG	$C_{X\alpha^2}$	12.6	*
NORMAL FORCE	$C_{N\alpha}$	8.28	25.4
STATIC MOMENT	$C_{m\alpha}$	−16.0	2.5
CUBIC STATIC MOMENT	$C_{m\alpha^3}$	1700.0	FROM PREVIOUS DATA
PITCH DAMPING MOMENT	$C_{mq} + C_{m\dot{\alpha}}$	170.0	*
TRIM ANGLE	α_0	0.09 (deg)	10.
STATIC MARGIN	ΔX_{cp}	8.3%	*

NOTE: 6 DOF REDUCTION

Unfortunately, as in Phase I, no fit could be obtained that gave a negative pitch-damping coefficient, and the static-moment coefficient again proved to be nonlinear. Figure 25 clearly shows that the round was launched at very low yaw and this yaw continuously increased along the range trajectory. As before, the round is passing through roll yaw resonance (Figure 26); however, the absolute roll rate is less than that observed in Phase I. This would seem to indicate that the threads on the Phase I design probably controlled the roll rate. Again, the authors express no confidence in the pitch-damping moment coefficient for the same reasons stated in the earlier discussion of the Phase I results. Enough quality trajectory data is not available to completely extract the nonlinear characteristics of this configuration.

Table 6 gives the results of the data fits for the cruciform fin-stabilized configuration (round nos. 20514 and 20515). The data resembles a conventional KE round. There are no nonlinear stability derivatives, the static margin is much larger than any of the fluted flare penetrators tested, and the pitch-damping moment is negative. These facts are confirmed by the data shown in Figures 27, 28, and 29. In Figure 27, a plot of pitch (α) and yaw (β) vs. range for round no. 20515, the initial yaw is low and it
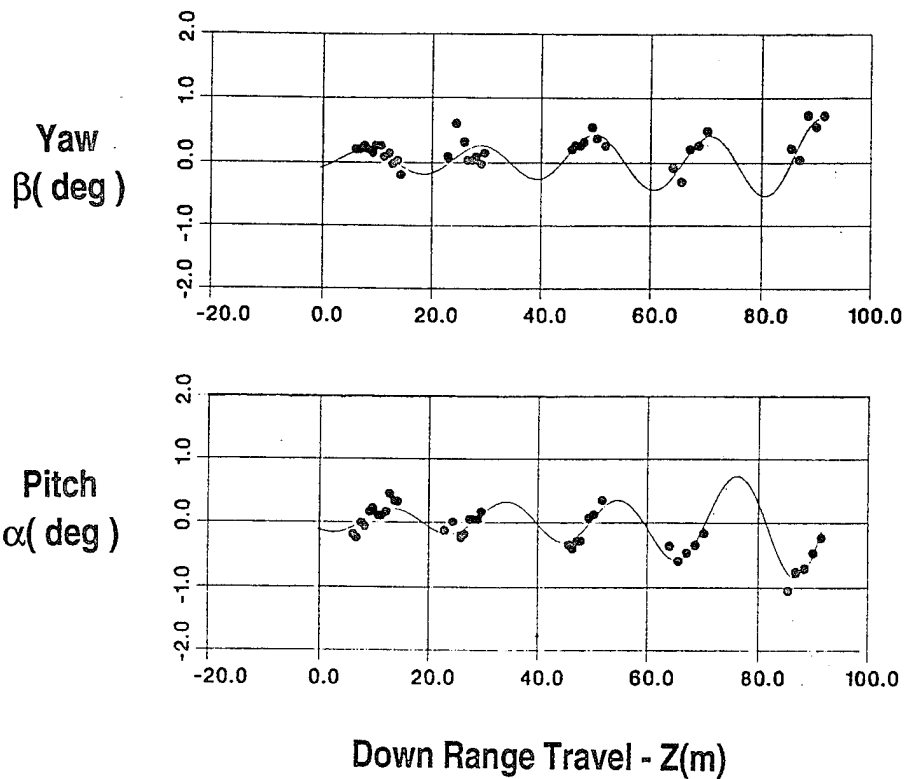
Figure 25. Angular trajectory motion fit; yaw and pitch (round no. 20511).

Table 6. Data Fit Results Round No. 20514 and Round No. 20515

COEFFICIENT	SYMBOL	VALUE (20514)	ERROR (%)	VALUE (20515)	ERROR (%)
AXIAL FORCE	C_x	0.38	1.3	.37	1.3
YAW DRAG	$C_{X\alpha}{}^2$	*	*	*	*
NORMAL FORCE	$C_{N\alpha}$	5.2	9.6	4.5	14.0
STATIC MOMENT	$C_{m\alpha}$	−19.7	1.5	−19.2	0.7
CUBIC STATIC MOMENT	$C_{m\alpha}{}^3$	*	*	*	*
PITCH DAMPING MOMENT	$C_{mq} + C_{m\alpha}$	−566.0	30.2	−317.	26.0
TRIM ANGLE	α_0	0.28 (deg)	7.5	0.07 (deg)	34.0
STATIC MARGIN	ΔX_{cp}	16.5%	*	18.6%	*

NOTE: 6 DOF REDUCTION

30

Figure 26. Vehicle roll rate vs. range (round no. 20511).

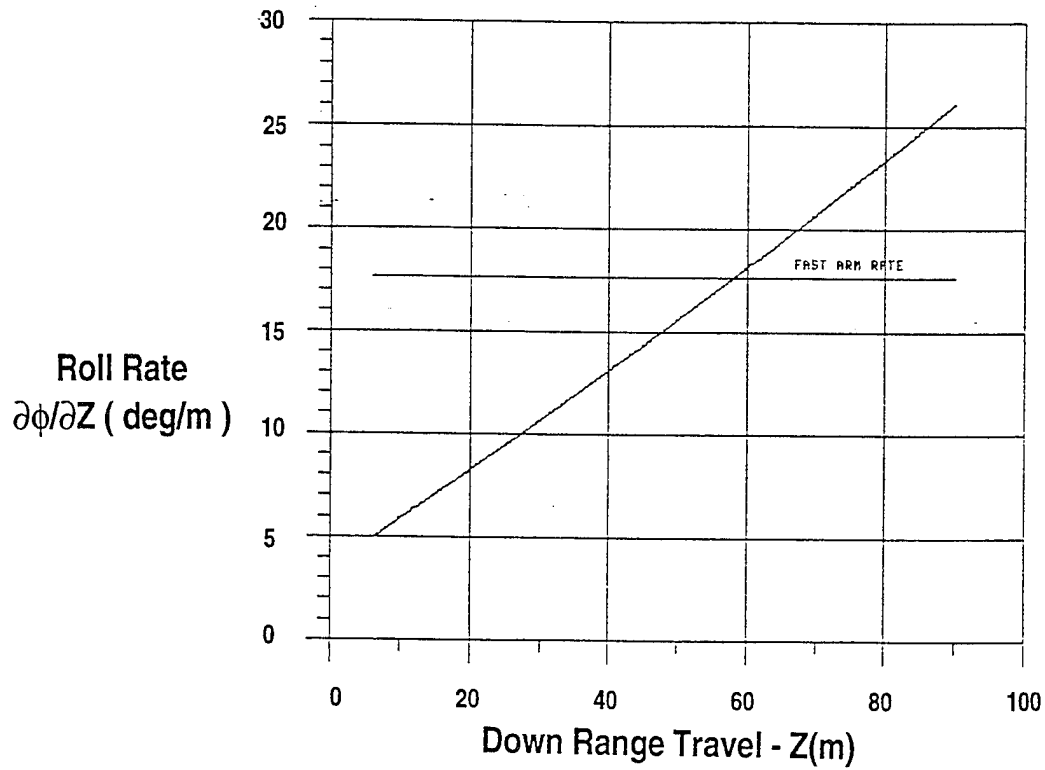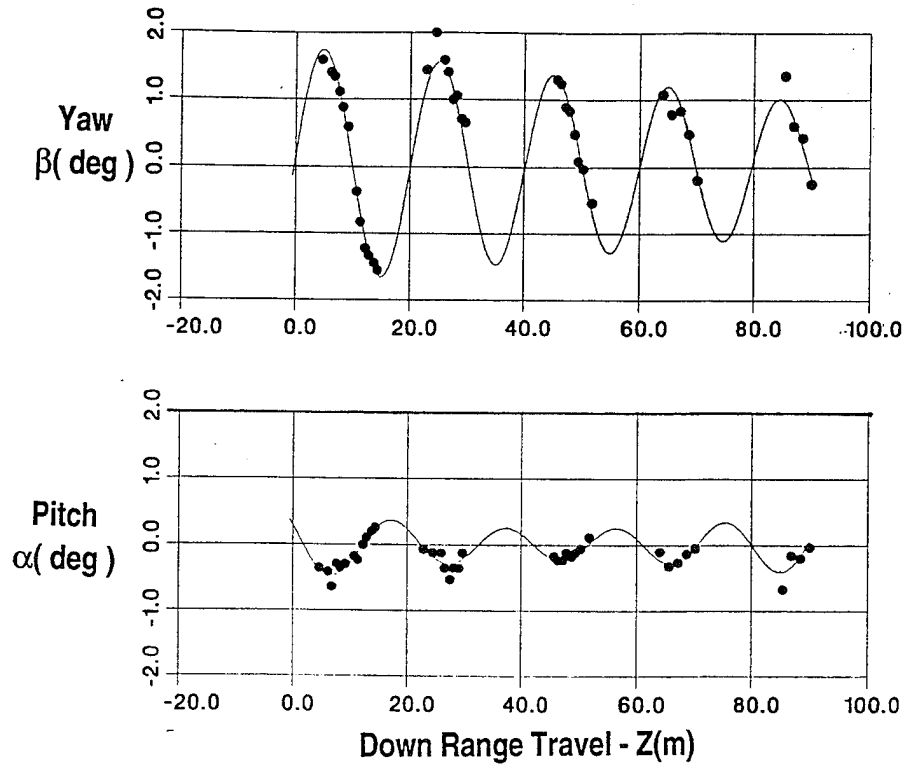Figure 27. Angular trajectory motion fit; yaw and pitch (round no. 20515).

31
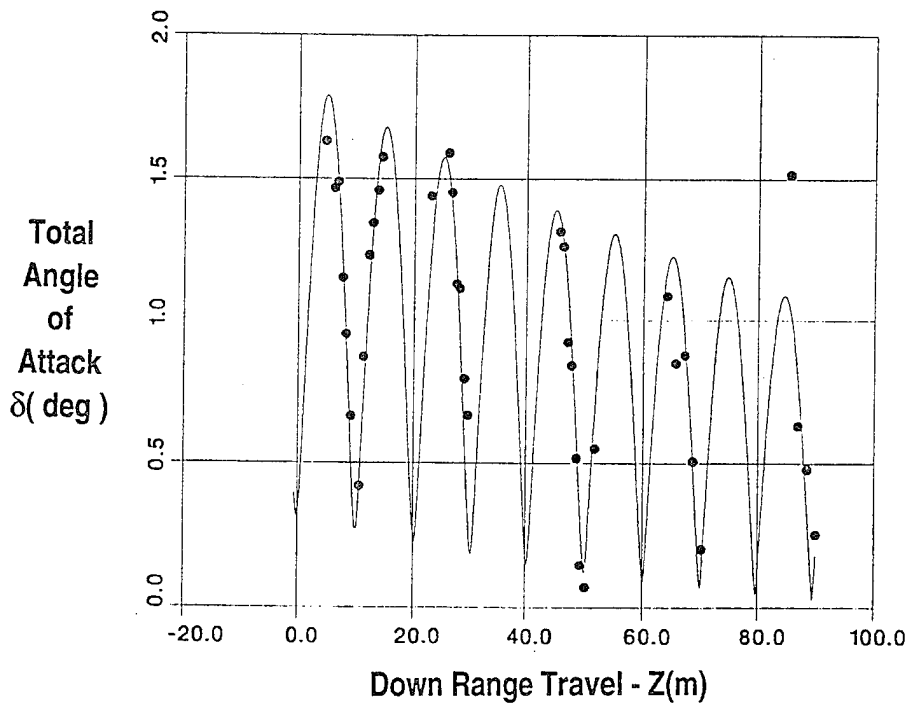
Figure 28. Total angle of attack vs. range (round no. 20515).
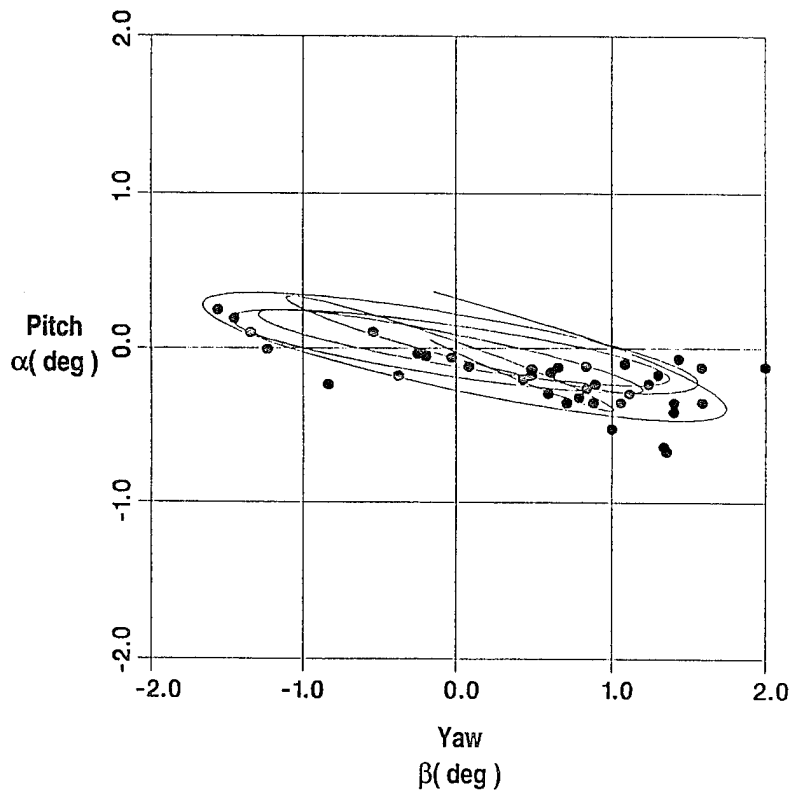
Figure 29. Pitch vs. yaw (round no. 20515).

diminishes with range. This is clearly reinforced in Figure 28, total angle of attack vs. range, and Figure 29, a plot of complex yaw. The roll history and roll rate for round no. 20515 are provided in Figures 30 and 31, respectively. The round is not at roll yaw resonance within the confines of the range trajectory. The roll rate is much lower than that observed for any of the fluted flare configurations during any phase of the testing.

It is obvious that the cruciform tail configuration is the classic example of a linear statically and dynamically stable fin-stabilized KE penetrator. The drag is a little larger than the drag of the fluted flare configuration. Referring back to Figures 23 and 24, it can be seen that the grooves still generate a significant viscous layer, but more of the fin surfaces are in the high-energy free stream. This accounts for the higher drag, but definitely provides stability and reduced aerodynamic jump sensitivity. Because accuracy is essential, the cruciform fin-stabilized configuration became the round of choice for the CCEMG program.

The full-scale cruciform tail design has a smaller nose radius in order to reduce drag. The small nose radius will shift the center of pressure forward relative to that of the subscale design. This is offset by the tungsten/titanium mass distribution center-of-gravity location that is further forward on the body. If even more static margin is required in the full-scale design, the nose radius can be increased with the attendant penalty in drag.

6. SUMMARY AND CONCLUSIONS

A fluted flare-stabilized penetrator and a cruciform fin-stabilized penetrator were tested to determine their aeroballistic characteristics. The fin-stabilized penetrator had the aerodynamic performance most consistent with the requirements of the CCEMG program and was selected for the program. The full-scale version of the penetrator has been successfully fired from the CCEMG cannon at velocities of 1,750 m/s. Figure 32 shows the muzzle x-rays taken 0.5 m downrange showing the initial vertical and horizontal separation of the armature/sabot from the fin-stabilized penetrator. This is the first time an ordnance configuration has been fired from an EM gun in the United States, has hit at zero yaw, and has penetrated armor targets over 225 m downrange!
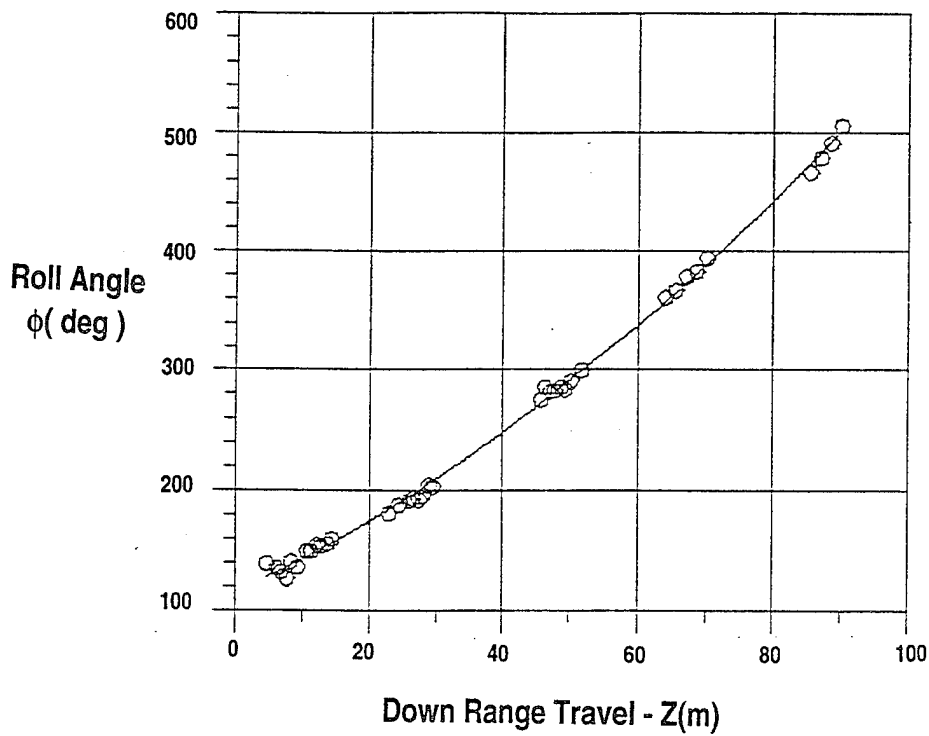
Figure 30. Vehicle roll angle vs. range (round no. 20515).
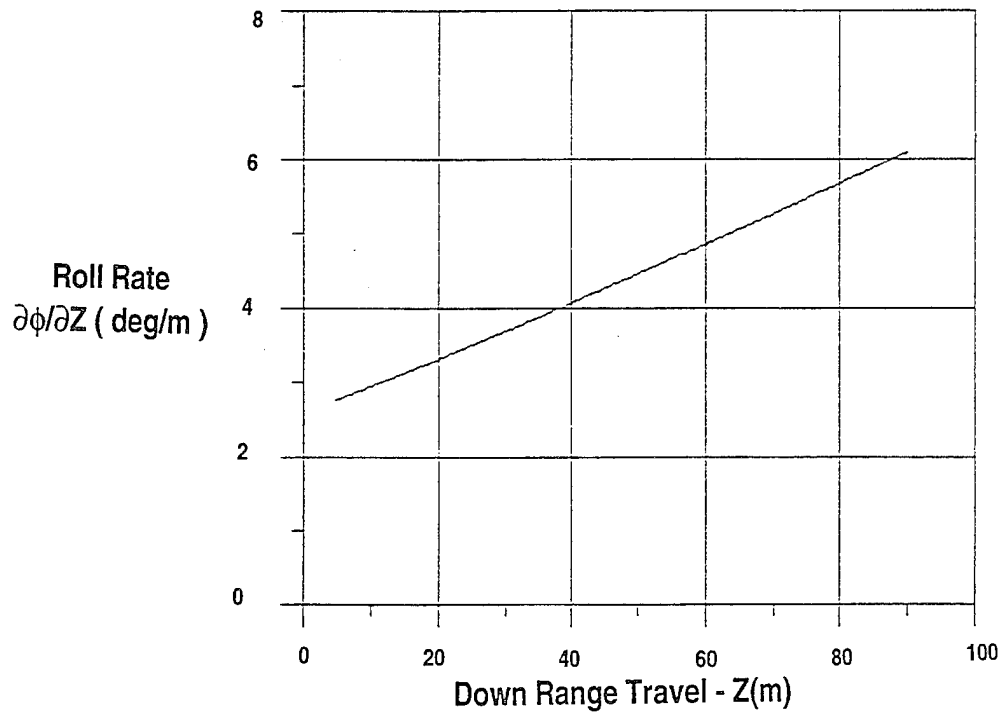
Figure 31. Vehicle roll rate vs. range (round no. 20515).

34

HORIZONTAL VIEW
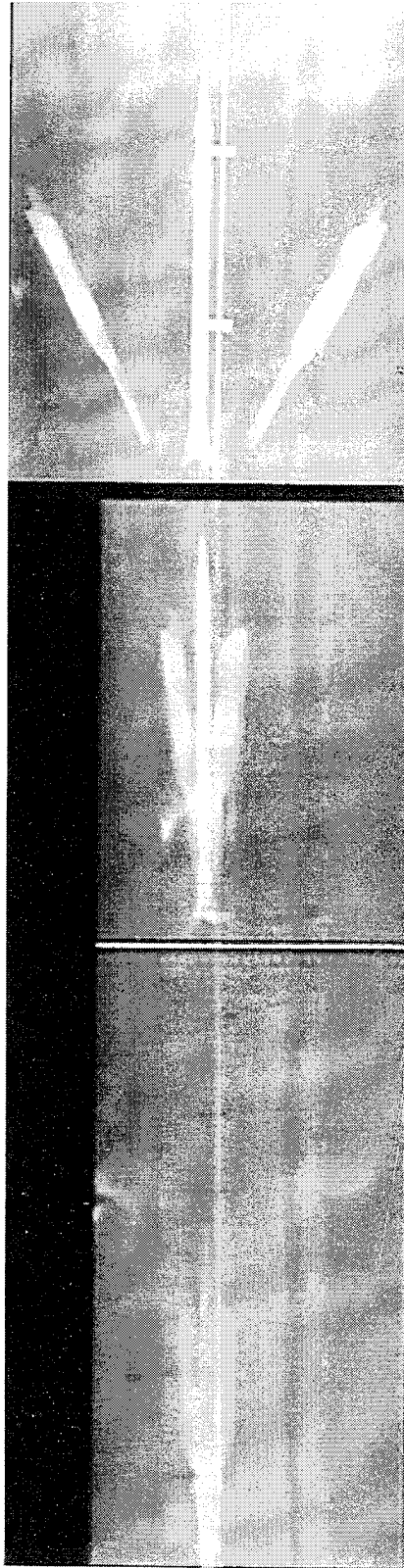
VERTICAL VIEW

Figure 32. X-rays of EM gun launch sabot/armature discard (V = 1,750 m/s).

35

INTENTIONALLY LEFT BLANK.

7. REFERENCES

Anderson, R. D., and K. D. Fickie. "IBHVG2 - A User's Guide." BRL-TR-2829, U.S. Army Ballistic Research Laboratory, Aberdeen Proving Ground, MD, July 1987.

Bornstein, J., I. Celmins, P. Plostins, and E. M. Schmidt. "Launch Dynamics of Fin-Stabilized Projectiles." Journal of Spacecraft and Rockets, vol. 29, no. 2, pp. 166–172, March–April 1992.

Braun, W. F. "The Free Flight Aerodynamics Range." BRL-R-1048, U.S. Ballistic Research Laboratory, Aberdeen Proving Ground, MD, July 1958.

Hathaway, W. H., and R. H. Whyte. "Aeroballistic Research Facility Free Flight Range Data Analysis Using the Maximum Likelihood Method." AFATL-TR-79-98, U.S. Air Force Armament Laboratory, Eglin Air Force Base, FL, December 1979.

Murphy, C. H. "The Free Flight Motion of Symmetric Missiles." BRL-TR-1216, U.S. Army Ballistic Research Laboratory, Aberdeen Proving Ground, MD, July 1963.

Plostins, P., I. Celmins, J. Bornstein, and J. E. Deibler. "The Effect of Front Borerider Stiffness on the Launch Dynamics of Fin-Stabilized Kinetic Energy Ammunition." BRL-TR-3057, U.S. Army Ballistic Research Laboratory, Aberdeen Proving Ground, MD, October 1989.

Plostins, P., J. Bornstein, and I. Celmins. "The Effect of Sabot Wheelbase and Position on the Launch Dynamics of Fin-Stabilized Kinetic Energy Ammunition." BRL-TR-3225, U.S. Army Ballistic Research Laboratory, Aberdeen Proving Ground, MD, April 1991.

INTENTIONALLY LEFT BLANK.

LIST OF SYMBOLS

C_{lp}	=	roll damping coefficient
$C_{l\delta}$	=	roll torque coefficient
C_m	=	total static moment coefficient
$C_{m\alpha}$	=	static moment coefficient
$C_{m\alpha^3}$	=	cubic static moment coefficient
$C_{m\alpha^5}$	=	quintic static moment coefficient
$C_{mq} + C_{m\dot{\alpha}}$	=	pitch damping coefficient
$C_{N\alpha}$	=	normal force coefficient
C_x	=	axial force coefficient
$C_{m\alpha^2}$	=	axial yaw drag coefficient
d	=	projectile reference diameter (m)
I_x	=	axial moment of inertia (kg-m^2)
I_y	=	transverse moment of inertia (kg-m^2)
m	=	projectile mass
ΔX_{cp}	=	projectile static margin (% length)
X	=	horizontal travel (m)
Y	=	vertical travel (m)
Z	=	downrange travel (m)

Greek

α	=	angle of attack (pitch) (deg)
α_o	=	trim angle of attack (deg)
β	=	angle of side slip (yaw) (deg)
δ	=	total angle of attack (deg)
ϕ	=	roll angle (deg)

INTENTIONALLY LEFT BLANK.

NO. OF
COPIES   ORGANIZATION

2   DEFENSE TECHNICAL INFO CTR
     ATTN DTIC DDA
     8725 JOHN J KINGMAN RD
     STE 0944
     FT BELVOIR VA 22060-6218

1   DIRECTOR
     US ARMY RESEARCH LAB
     ATTN AMSRL OP SD TA
     2800 POWDER MILL RD
     ADELPHI MD 20783-1145

3   DIRECTOR
     US ARMY RESEARCH LAB
     ATTN AMSRL OP SD TL
     2800 POWDER MILL RD
     ADELPHI MD 20783-1145

1   DIRECTOR
     US ARMY RESEARCH LAB
     ATTN AMSRL OP SD TP
     2800 POWDER MILL RD
     ADELPHI MD 20783-1145

     ABERDEEN PROVING GROUND

5   DIR USARL
     ATTN AMSRL OP AP L (305)

NO. OF COPIES	ORGANIZATION	NO. OF COPIES	ORGANIZATION
2	COMMANDER US ARMY ARDEC ATTN SMCAR FSA E DR T GORA JOHN BENNETT PCNTY ARSNL NJ 07806-5000	1	COMMANDER US ARMY ARDEC ATTN SMCAR FSF GD MR K PFLEGER PCNTY ARSNL NJ 07806-5000
4	COMMANDER US ARMY ARDEC ATTN SMCAR CCL FA H MOORE LTC GERASIMAS W WILLIAMS B SCHLENNER BLDG 65N PCNTY ARSNL NJ 07806-5000	5	COMMANDER US ARMY ARDEC ATTN SMCAR FSF BV MR V GALGANO MR C GONZALES MR C LANGEN MR E DELCOCO MR C CORDING PCNTY ARSNL NJ 07806-5000
1	HQDA ATTN SARD TT DR F MILTON WASH DC 20310-0103	1	COMMANDER US ARMY YPG ATTN STEYP MTW YUMA AZ 85365-9103
1	HQDA ATTN SARD TT DR J APPEL WASH DC 20310-0103	9	COMMANDER US ARMY TMAS ATTN AMCPM TMA MR D GUZIEWICZ
2	COMMANDER US ARMY ARDEC ATTN SMCAR AET A MR J GRAU MR C NG PCNTY ARSNL NJ 07806-5000		MR K RUBEN MR C KIMKER MR R JOINSON MR A HYDER MR E KOPOAC MAJ R BILLINGTON MAJ B HELD PCNTY ARSNL NJ 07806-5000
15	COMMANDER US ARMY ARDEC ATTN SMCAR CCH MR J DELORENZO MR E FENNELL MR P CHRISTAN MR S MUSALLI MR B KONRAD MR F RENNER MR R SAYER MR P DONADIO MR R CARR MR K FEHSAL MR S GHASI MR E LOGSDON MR N KRASNOW MR T LOUZERIO MR M PALATHINGAL PCNTY ARSNL NJ 07806-5000	11	COMMANDER US ARMY TACOM ATTN AMCPEO HFM AMCPEO HFM F AMCPEO HFM C AMCPM ABMS AMCPM BLOCKIII AMSTA CF AMSTA Z AMSTA ZD AMCPM ABMS S W DR PATTISON MR A HAVERILLA WARREN MI 48397-5000

NO. OF COPIES	ORGANIZATION	NO. OF COPIES	ORGANIZATION
1	COMMANDER US ARMY TACOM ATTN SFAE ASM AB SW M KAHN WARREN MI 48397-5000	1	NAVAL ORDNANCE STATION ADVNCD SYS TECHLGY BR ATTN DAN HOLMES CODE 2011 LOUISVILLE KY 40214-5001
1	COMMANDER USAOTEA ATTN CSTE CCA DR RUSSELL ALEXANDRIA VA 22302-1458	1	NSWC DAHLGREN DIV ATTN DR F G MOORE CODE G04 DAHLGREN VA 22448-5000
2	DIRECTOR USA ARMOR CTR & SCHOOL ATTN ATSB WP ORSA A POMEY ATSB CDC FORT KNOX KY 40121	3	CG MCRDAC CODE AWT ATTN DR C VAUGHN MR G SOLHAND MAJ F WYSOCKI QUANTICO VA 22134-5080
1	COMMANDER AMCCOM ATTN AMSMC ASR A MR CRAWFORD ROCK ISLAND IL 61299-6000	2	PM GROUND WEAPONS MCRDAC ATTN LTC VARELA CBGT QUANTICO VA 22134-5000
1	COMMANDER AMCCOM ATTN AMSMC QAT A D R SCHUBERT PCNTY ARSNL NJ 07806-5000	1	WL MNSH SITE A 15 ATTN DONALD M LITTRELL EGLIN AFB FL 32542-5434
2	COMMANDER JEFFERSON PROV GRND ATTN STEJP TD MADISON NJ 47250-5100	2	DIRECTOR BENET LABS ATTN SMCAR CCB RT M CIPOLLO SMCAR CCB RM P VOTTIS WATERVLIET NY 12189
4	COMMANDER US ARMY TRADOC ATTN ATCD T ATCD TT ATTE ZC ATTG Y FORT MONROE VA 23651-5000	1	DIRECTOR LLNL ATTN DR R S HAWKE L 153 PO BOX 808 LIVERMORE CA 94550
1	NAWC CODE C2774 CLPL ATTN FRANK PICKETT BLDG 1031 CHINA LAKE CA 93555	2	DIRECTOR BENET LABS ATTN SMCAR CCB W KITCHENS L JOHNSON WATERVLIET NY 12189-5000

NO. OF COPIES	ORGANIZATION
1	DIRECTOR BENET LABS ATTN SMCWV QAR T MCCLOSKEY WATERVLIET NY 12189-5000
3	DIRECTOR SANDIA NATIONAL LABS ATTN A HODAPP W OBERKAMPF F BLOTTNER DIVISION 1631 ALBUQUERQUE NM 87185
1	AUBURN UNIV ATTN DR E CLOTHIAUX 206 ALLISON LAB AUBURN UNIV AL 36849-5311
1	TEXAS TECHL UNIV DEPT OF EE CMPTR SCIENCE ATTN DR M KRISTIANSEN LUBBOCK TX 79409-4439
5	INST FOR ADVANCED TECHLGY THE UNIV OF TX AT AUSTIN ATTN DR HARRY FAIR DR KUO TA HSIEH DR IAN MCNAB MR PATRICK SULLIVAN DR WILLIAM REINECKE 4030 2 W BRAKER LANE AUSTIN TX 78759-5329
1	UNIV OF MIAMI DEPT OF PHYSICS ATTN DR M A HUERTA PO BOX 248046 CORAL GABLES FL 33124
1	NCSU DEPT OF NUCLEAR ENGRG ATTN DR JOHN GILLIGAN PO BOX 7909 RALEIGH NC 27695
1	UNIV OF TENNESSEE ATTN DR DENNIS KEEFER SPACE INST MAIL STOP 14 B H GOETHERT PRKWY TULLAHOMA TN 37388-8897

NO. OF COPIES	ORGANIZATION
3	UNIV OF TX AT AUSTIN ATTN MR S B PRATAP MR J H PRICE DR HEEDO YUN 10100 BURNET RD BLDG 133 AUSTIN TX 78748
1	GA TECHNOLOGIES INC ATTN DR L HOLLAND PO BOX 85608 SAN DIEGO CA 92138
1	ELECTROMAGNETIC RSRCH INC ATTN DR PETER MONGEAU 2 FOX RD HUDSON MA 01749
2	LAP RESEARCH INC ATTN DR JOHN P BARBER MR DAVID P BAUER 2763 CULVER AVE DAYTON OH 45429-3723
2	SAIC ATTN DR K A JAMISON DR GLENN ROLADER 1247 B N EGLIN PRKWY SHALIMAR FL 32579
1	UDLP MAILSTOP M170 ATTN BRAD GOODELL 4800 E RIVER RD MINNEAPOLIS MN 55421-1498
2	SAIC ATTN DR JAD H BATTEH MR L THORNHILL 1503 JHNSN FRY RD STE 100 MARIETTA GA 30062
1	WESTINGHOUSE SCIENCE AND TECHNOLOGY CENTER ATTN MR DOUG FIKSE 1310 BEULAH RD PITTSBURGH PA 15233
5	KAMAN SCIENCES CORP ATTN TIM HAYDEN 1500 GRDN OF THE GODS RD CO SPRINGS CO 80933-7463

NO. OF
COPIES   ORGANIZATION

1   LORAL VOUGHT SYSTEMS
        ATTN ROBERT TAYLOR
        PO BOX 650003 WT
        DALLAS TX 75265-0003

2   ALLIANT TECHSYSTEMS
        ATTN C CANDLAND
        R BECKER
        7225 NORTHLAND DR
        BROOKLYN PARK MN 55428

2   ARROW TECH ASSOCS INC
        ATTN MR R WHYTE
        MR W HATHAWAY
        PO BOX 4218
        S BURLINGTON VT 05401-0042

        ABERDEEN PROVING GROUND

49   DIR USARL
        ATTN   AMSRL WT I MAY
               AMSRL WT W C MURPHY
               AMSRL WT WB
                 F BRANDON
                 W D'AMICO
               AMSRL WT WC J ROCCHIO
               AMSRL WT T W F MORRISON
               AMSRL WT TC
                 W DE ROSSET
                 R COATES
               AMSRL WT P A HORST
               AMSRL WT PA T MINOR
               AMSRL WT PB
                 P PLOSTINS (13 CP)
                 E SCHMIDT
                 M BUNDY
                 K SOENCKSEN (10 CP)
                 D WEBB
                 D SAVICK
                 V OSKAY
                 A ZIELINSKI
               AMSRL WT PD
                 T ERLINE
                 B BURNS
                 L BURTON
                 R KASTE
                 S WILKERSON
                 K BANNISTER
                 W DRYSDALE
                 A DRYDMAN
                 T LI
               AMSRL HR M G L HORLEY

INTENTIONALLY LEFT BLANK.

USER EVALUATION SHEET/CHANGE OF ADDRESS

This Laboratory undertakes a continuing effort to improve the quality of the reports it publishes. Your comments/answers to the items/questions below will aid us in our efforts.

1. ARL Report Number __ARL-TR-922_____ Date of Report __January 1996_____

2. Date Report Received _____

3. Does this report satisfy a need? (Comment on purpose, related project, or other area of interest for which the report will be used.) _____

_____

_____

4. Specifically, how is the report being used? (Information source, design data, procedure, source of ideas, etc.) ____

_____

_____

5. Has the information in this report led to any quantitative savings as far as man-hours or dollars saved, operating costs avoided, or efficiencies achieved, etc? If so, please elaborate. _____

_____

_____

6. General Comments. What do you think should be changed to improve future reports? (Indicate changes to organization, technical content, format, etc.) _____

_____

_____

_____

_____
Organization

CURRENT
ADDRESS
_____
Name

_____
Street or P.O. Box No.

_____
City, State, Zip Code

7. If indicating a Change of Address or Address Correction, please provide the Current or Correct address above and the Old or Incorrect address below.

_____
Organization

OLD
ADDRESS
_____
Name

_____
Street or P.O. Box No.

_____
City, State, Zip Code

(Remove this sheet, fold as indicated, tape closed, and mail.)
(DO NOT STAPLE)